TID-4500, UC-34
Physics

LAWRENCE LIVERMORE LABORATORY
University of California/Livermore, California/94550

UCRL-51109

THE USE OF SHOCK WAVES IN THE VAPORIZATION OF METALS

Thomas J. Ahrens
Parl A. Urtiew

MS. date: August 5, 1971

Contents

THE USE OF SHOCK WAVES IN THE VAPORIZATION OF METALS

Abstract

Explosively induced shock waves in aluminum, iron, stronium, lithium, thorium, uranium, and barium are capable of vaporizing appreciable quantities of these metals. When plane shock waves are incident upon porous samples, they will induce vaporization in aluminum, iron, strontium, thorium, and barium. Although Mach stem shocks act on a smaller selective mass of material, they will induce sufficient entropy to vaporize uranium and lithium. When a Mie-Grüneisen equation of state is assumed, it is found that for a given plane explosive system an initial porosity exists that will optimize the shock-induced entropy production in a metal. The optimum initial distention that will result in maximum post-shock entropy is found to vary between 1.6 and 2.0 times the volume of the crystal for several of the metals examined.

Introduction

The possible use of explosively induced shock waves to produce large masses of vaporized metal is examined in this report. Shock-wave induction of metal gas appears to be a relatively simple method for releasing various metal species in the upper atmosphere from ionospheric sounding rockets. Observations of the reactions that take place between the metallic species and the ambient atmospheric species, and of the relative populations of species that result from such metallic vapor releases, can be made using either airborne or ground-based spectroscopic instruments.

The high available energy density of military high explosives (1 kcal/g), as well as the relative ease with which a large fraction of this energy density (approximately 20%) may be imparted to a metal target, make the possible application of the shock-wave method for the sudden production of metal vapor a potentially attractive technique. In addition to the intrinsic thermal (random direction) velocities imparted to the resulting high-entropy gas cloud, the shock interaction and following rarefaction wave will induce a net flow field (with peak velocities of approximately 10 km/sec) in the gas cloud. High explosives may be employed in this context in either one-dimensional plane-wave or dimensional Mach-stem geometries. In the plane-wave geometry the explosive can be detonated in contact with the

sample, thus directly imparting a shock wave to the metal; or plane-flowing detonation gases can accelerate a flyer plate, which in turn may be used to shock the sample upon impact. As is demonstrated in the next section, the plane technique is simpler and it can vaporize metals such as iron, thorium, strontium, barium, and aluminum. However, metals such as lithium and uranium are difficult to vaporize by this technique. For these metals the Mach-stem method appears to be the only one available, and it has the limitation that it vaporizes less material.

A Mach stem is a shock discontinuity that is formed when two shock waves approach each other at an angle. If the angle between the wave fronts is zero, a simple head-on collision of shocks occurs that produces high temperatures and vaporization, but no net flow of the induced gas. By increasing the incidence angle, regular oblique reflection will take place until some angle is reached where reflection becomes irregular and Mach-stem reflection begins.

The purpose of this report is to provide design criteria for the construction of shock-vaporization experiments. Specifically, the report examines pertinent experimental parameters, and it provides some design data used to select initial porosities, types, and speeds for explosively driven plates and Mach stems. The driver plates and Mach stems are capable of inducing shocks that will either completely or partially vaporize aluminum, iron, lithium, barium, strontium, thorium, and uranium.

Plane-Wave Vaporization

For the following calculations it is assumed that a quantity of an explosive such as 9404 (plastic bonded HMX) is plane-detonated to accelerate a flyer plate to speeds in the 4 to 5 km/sec range (see Fig. 1). The flyer plate either impacts the metal to be vaporized directly, or it impacts an impedance-matching driver plate upon which the sample is placed. In determining the conditions required for vaporization as a result of shock compression and subsequent rarefaction, it is assumed that all the entropy production results only from the shock compression process. In essence then, it is assumed that the rarefaction process is isentropic. In principle it is possible that the total entropy within a control volume could increase during the rarefaction process (and the process remain strictly adiabatic); however, it is assumed that any increase in entropy upon

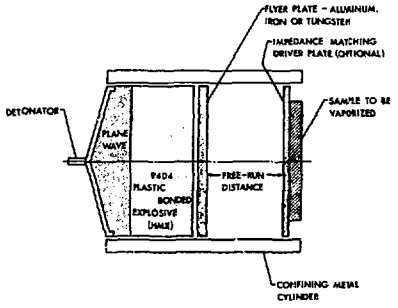

Fig. 1. Shot assembly for the plane-wave experiment.

rarefaction will be small compared to the shock-induced entropy.

Thus the tactic followed is to calculate the entropy increase resulting from shock compression of both initially single-crystal density and initially porous metals. Entropy production in porous metals is investigated because, although for a given explosive system the maximum shock pressure that may be achieved is lower than that achievable in a similar sample, with initially single-crystal density the specific entropy production may under certain conditions be greater than for the solid sample. Since we are assuming that, upon rarefaction from the high pressure shock state, entropy is conserved (isentropic release), the entropy increase with temperature near or at ambient pressure is also calculated. Of specific interest are the values of the entropy of the liquid metal at the point of incipient boiling, i.e., the start of vaporization, and the entropy for complete vaporization. According to arguments given by Zeldovich and Raizer,[1] the internal energy achieved by the metallic elements in the region of the vapor-liquid critical point are on the order of twice their binding energy. From this they conclude that metals achieving entropies appropriate to this state will, upon expansion, ultimately be completely vaporized. Therefore, by equating calculated

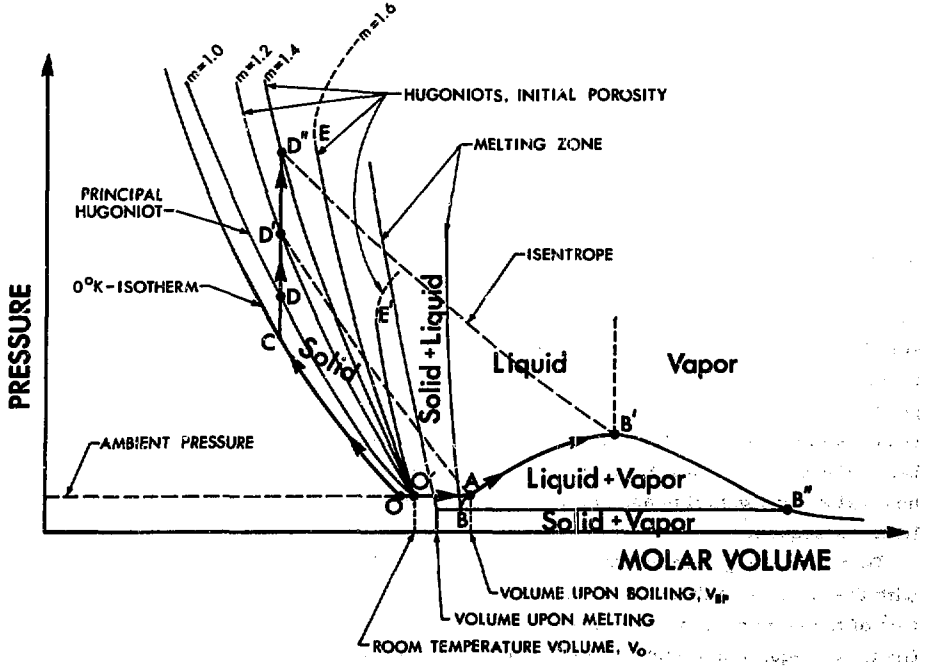

Fig. 2. Thermodynamic diagram representing various paths for vaporization.

entropies in the high-pressure shock state with those achieved by increasing the temperature at ambient pressure, the range of states in the solid that have sufficient entropy to result in incipient, partial, or complete vaporization upon isentropic pressure release may be determined.

The behavior upon being shocked to high pressure of a metal with various initial porosities is illustrated in Fig. 2. When samples initially having the single-crystal molar volume, point $0'$, are singly shocked, they achieve states such as D along the principal Hugoniot curve (m = 1.0). At a given molar volume, V, Hugoniots of porous samples (initial volume, mV_0) will generally lie above the principal Hugoniot. Hypothetical release isentropes from states having sufficient entropy to induce incipient and substantial vaporization are indicated by D'A and D"B', respectively. In general, explicit knowledge of the release isentropes are not required; only knowledge of the entropy associated with points connected by the isentrope passing through a Hugoniot state and a high-temperature, low-pressure state is of interest.

Calculation of Entropy Upon Shocking Solid and Porous Metals

In the present calculations, initial equation-of-state data in the form of smoothed principal Hugoniot curves and calculated shock temperatures are assumed. Several nearly equivalent methods for smoothing experimental Hugoniot data and carrying out the shock temperature calculations have been reported, e.g., Zeldovich and Raizer,[1] Rice et al.,[2] and Walsh and Christian.[3] In addition, the Debye model is assumed to describe the solid's thermal properties at temperatures substantially below the Debye temperature. However, over most of the temperature range of interest, the solid has achieved the Dulong-Petit specific heat value, and thus this assumption is of little consequence.

To relate changes in thermal pressure with the changes in thermal energy content of the compressed solid, the Mie-Grüneisen equation of state is assumed. Thus γ, the Grüneisen parameter is given by

$$\gamma = V\left(\frac{\partial p}{\partial E}\right)_V , \qquad (1)$$

where p is pressure and E is internal energy. The assumption that

$$\gamma = \gamma(V) \qquad (2)$$

is demonstratively inadequate, particularly at very high shock-induced temperatures. Although in the present report we employ only the assumption embodied by Eq. (2), we discuss the difficulty that arises from this assumption later in this section.

In the calculation of shock-induced entropy production we employ, at each volume, the Dugdale-MacDonald (Grover et al.[4]) values of γ where it has been specified in the published reduction of the Hugoniot data. For several metals where $\gamma(V)$ is not explicitly given, we used the assumption that γ/V remains a constant with compression; the zero-pressure

value of this quantity is adopted. In any case we use this assumption to estimate the variation of the Debye temperature, θ, with compression. We note that if the Debye model for the phonon spectral density is assumed, it follows that

$$\gamma = -\partial \ln \theta / \partial \ln V, \qquad (3)$$

which upon integration yields

$$\theta = \theta_0 \exp[\gamma(1 - V/V_0)], \qquad (4)$$

where θ_0 and V_0 are the Debye temperature and molar volume at the reference state. In order to calculate entropy at Hugoniot points such as D, D' and D'' (Fig. 2), it is convenient to initially calculate the entropy along the principal Hugoniot, O'D via the thermodynamic path, O'OCD. This calculation is straightforward, as the entropy increase along OC—the 0°K isotherm—is zero by the third law. Thus the entropy increase occurs only at constant volume along CD and is given by

$$dS_{CD} = \int_0^{T_h} \frac{C_V(\theta/T)}{T} dT, \qquad (5)$$

where C_V is the specific heat at constant volume. Since the results of this integral for a Debye solid are tabulated by Furukawa and Douglas,[5] in practice a simple look-up and interpolation routine is employed (see the appendix). Shock temperatures, T_h, for each metal studied, have been taken from the literature and are given later in the section on "Entropy Production in Porous Metals by Plane Shocks." Alternately, the entropy increase along CD can be calculated from the empirical formula (derived from the Debye model)

$$S_{CD} = 5.9587 \left\{ \ln(T_h/\theta) + 1.3296 + \frac{\theta}{T_h}\left[0.000322 + \frac{\theta}{T_h}\left(0.024386 + \frac{\theta}{T_h}\right.\right.\right.$$
$$\times \left\{0.0005943 + \frac{\theta}{T_h}\left[-0.0007624 + \frac{\theta}{T_h}\left(9.3 \times 10^{-5} - \frac{\theta}{T_h}\right.\right.\right.$$
$$\left.\left.\left.\left.\times 3.835 \times 10^{-6}\right)\right]\right\}\right)\Bigg]\Bigg\} \text{ cal/mole °K}. \qquad (6)$$

For shock temperatures greater than 10, we assume a value for C_V of 3R (where R is the gas constant). The entropy increase is then given by

$$\Delta S_{CD} = 21.65 + 3R \ln \times (T_h/10\theta) \text{ cal/mole °K}, \qquad (7)$$

where the constant 21.65 is the entropy at $10(\theta/T)$. As can be seen in Tables 3 and 4, the calculated entropies along the principal Hugoniot for aluminum and iron are very close to those that were calculated by a fundamentally equivalent procedure by McQueen et al.[6] for similar-density iron and aluminum alloys. Probably due to the marked dilution of uranium by molybdenum (refer to Table 7), the agreement between the present uranium calculation and the results for U/Mo is relatively poor.

To calculate the Hugoniot pressures achieved at a given molar volume by metals with different initial porosities, we employ the Rankine-Hugoniot equation for conservation of energy,

$$E_x = E_0 + \frac{1}{2} p_x (mV_0 - V), \qquad (8)$$

and the Mie-Grüneisen equation,

$$P_x - p_y = \frac{\gamma}{V}(E_x - E_y), \qquad (9)$$

where E_x and p_x, and E_y and p_y are the internal energies and shock pressures associated with two shock states achieved

at the same molar volume. E_0 is the internal energy at the reference state, which for porous metals is assumed to be independent of initial porosity. Thus the surface energy associated with the initial distention of the sample is assumed to be negligible compared to the pertinent shock energies. We further assume that the porous metal is sufficiently fine-grained so that upon being encompassed by a shock, individual particles come to thermal equilibrium on a time scale comparable to the shock rise-time (approximately 0.01 μsec). Also implicit in this formulation is the assumption that the shock pressures of interest greatly exceed the crushing strength of the initial sample pore structure.

If a porous sample with an initial molar volume m_0V_0 is shocked to a specific volume, V, the resulting Hugoniot pressure, p_m, is related to the pressure along the principal Hugoniot, p_h, at the same volume by

$$p_m = p_h \left\{ 1 + \frac{(m - 1)V_0}{V} \times [2\gamma - mV_0/V + 1]^{-1} \right\} . \qquad (10)$$

In the case where the material of interest has a very large initial distention, a problem arises in the calculation of the Hugoniot at such points as E and E' (see Fig. 2). At these points the Hugoniot assumes a slope of $-\infty$, and at higher pressures the shock pressure becomes double valued with respect to volume. In general this situation will occur at pressures above which the condition

$$m = \frac{V}{\gamma V_0} = (2 + \gamma) \qquad (11)$$

is satisfied. Above this point the simple Mie-Grüneisen equation cannot be applied. As discussed earlier in this section, this has restricted our calculations to a lower range of porosities in several metals.

The shock temperature in the initially porous solid is related to the temperature along the principal Hugoniot at the same volume by

$$T_m = \frac{(p_m - p_h)V}{3\gamma R} , \qquad (12)$$

where we have assumed that above all principal Hugoniot temperatures of interest, the specific heat has assumed the Dulong-Petit value. Within this same assumption, at a given volume the increase in entropy of the initially porous sample is given by

$$S_{D-D'} = 3R \ln (T_m/T_h) . \qquad (13)$$

Calculation of Entropy Required for Vaporization

The entropy increase required to produce incipient vaporization (i.e., raise a metal to the boiling point) at standard pressure is given in Table 1, where it has been collected from data presented in several thermodynamic tabulations.[7-11] Generally the uncertainties in the entropies at ambient pressure are less than those calculated along the Hugoniot. Aside from experimental uncertainties in the shock data themselves, the major uncertainties in the Hugoniot entropies arise from the lack of direct knowledge of the high-pressure Grüneisen parameter and the degree to which the Mie-Grüneisen equation describes reality. Uncertainties

Table 1. Thermal properties of metals pertinent to shock-induced melting and vaporization.[a]

Element	Entropy at STP (cal/mol-°K)	Melting point: Temp (°K)	Melting point: Entropy, incipient melting (cal/mol-°K)	Melting point: Entropy, complete melting (cal/mol-°K)	Boiling point, 1 atm: Temp (°K)	Boiling point, 1 atm: Entropy, incipient boiling (cal/mol-°K)	Boiling point, 1 atm: Entropy, complete vaporization (cal/mol-°K)
Al	6.77	933	14.30	17.06	2793	25.38	50.98
Fe	6.52 7.106	1809	22.02	23.84	3135	29.89	56.54
Ba	14.92	1002	26.03	27.88	2171	35.45	51.03
Th	12.76	2028	29.18	31.08	5061	41.13	66.03
U	12.02	1405	27.04	28.49	4407	41.58	66.75
Pb	15.55	601	20.19	22.10	2023	30.60	51.59
Sr	12.50	1041	20.	24	1657	28	48
Li	7.00	454	9.67	11.25	1615	20.10	41.54

[a]Data were taken from Ref. 7 for all elements except Sr, whose data were taken from Ref. 9.

in the entropy along the Hugoniot, reflecting uncertainties in γ, are generally on the order of ±10%, but these can approach ±20% or more for large compressions, except for the case of aluminum and iron, for which high-pressure data for γ are reported (Anderson et al.[12]; McQueen et al.[6]).

The entropy increases upon being brought to the boiling point have only recently been determined in the case of barium and thorium. The values given in Table 1 are (except for the case of strontium) taken from the recent revision of the thermodynamic properties given by Hultgren et al.[7] We have used the entropy calculated for high temperatures at 1 atm realizing that this value will provide a moderate overestimate of the shock strength required to deliver metal gas in a vacuum.

Flyer Plate Impact Velocities Required for Shock Vaporization

The highest flyer plate velocities achievable by the suggested explosive system shown in Fig. 1 are in the 4-5 km/sec range, depending ultimately on the ratio of the mass per unit area of explosive to that of the flyer plate. A modest increase in velocity, to perhaps 6 km/sec, can probably be achieved by using the multiple-staging technique described by Balchan.[13] This latter technique will, of course, sharply reduce the total mass of the final flyer plate.

The shock entropies that can be achieved by either a single-stage technique (in which a high-impedance flyer plate, presumably tungsten or palladium, directly impacts the sample) or a simple system (using a driver plate of shock impedance intermediate between the flyer and sample) have been calculated and are discussed in the next section.

Entropy Production in Porous Metals by Plane Shocks

Theoretical Hugoniots for various initial sample porosities and the resulting entropies achieved with different flyer-plate systems are calculated using the relations given in the previous section with Fortran IV program ENT in the appendix. Although it is unlikely that aluminum flyer plates would be used for any optimum system, they are considered because the shock state induced by a 2024 aluminum flyer plate, impacting at a given velocity, closely approximates the free-surface velocity of an aluminum driver plate that might be used in a real system. Hugoniot data for the flyer plate materials, fitted to a third-order polynomial in the pressure-particle velocity plane are taken from the compilation of McQueen et al.[6]

The entropies, shock pressures, and shock particle velocities achieved along the principal and porous Hugoniots for aluminum, iron, thorium, uranium, strontium, and lithium are shown in Tables 2 through 8. Entropies achievable in each of these materials with 2024 aluminum, iron, or tungsten flyer (or, of course, driver) plates are shown in Figs. 3(a,b,c) to 9(a,b,c) as a function of initial distention. Hugoniot data for pure aluminum and pure uranium are inferred by correcting the data for 2024 alloy and U/Mo alloy (McQueen et al.[6]) for initial density. Data for thorium is reported by McQueen and Marsh.[14] Unpublished data (McQueen and Marsh) for barium and strontium was reduced by Rogers.[15] The reduction of the data of Rice,[16] carried out by Grover, is employed for lithium.

As can be seen in Figs. 3 through 9, it appears that, within the context of the Mie-Grüneisen theory, for a given flyer-plate material and impact velocity, an optimum initial porosity of the target exists, such that the shock-induced entropy is a maximum. In some cases the degree of initial porosity is critical (e.g., for aluminum and iron, Figs. 3 and 4) to the achievement of partial vaporization.

ALUMINUM

The results shown in Figs. 3(b) and 3(c) demonstrate that the optimum vaporization for 4- or 5-km/sec impacts is approximately $m = 1.6$ for iron and closer to $m = 1.7$ or $m = 1.8$ for tungsten flyer plates. However, only approximately 5% vaporization results from the impact of a 5-km/sec tungsten plate into a material for which $m = 1.6$. Calculations for larger initial porosities should be carried out above the point where the Hugoniot becomes double valued. This is outside the context of the Mie-Grüneisen assumption.

IRON

Similarly, optimum initial distentions required for vaporization for 4- to 5-km/sec iron and tungsten flyer plates (see Figs. 4(b) and 4(c)) are, respectively, $m = 1.6$ and 1.7. Vaporization is not achieved with a 5-km/sec aluminum flyer plate (see Fig. 4(a)). Approximately 10% vaporization is achieved upon the impact of a 5-km/sec plate into a material for which $m \approx 1.7$. The impact of an 8-km/sec plate will result in approximately 30% vaporization.

Table 2. Shock-wave parameters and thermodynamic states for pure aluminum.

Distention ratio (V_{00}/V_0)	Compression (V/V_0)	Shock pressure (Mbar)	Principal Hugoniot shock temp (°K)	Grüneisen ratio	Debye temp (°K)	Shock-particle velocity (km/sec)	Entropy[a] (cal/mol-°K)		Porous Hugoniot shock temp (°K)
1.0	0.9039	0.100	374.0	1.808	424.2	0.596	7.36	(7.18)	374.0
1.2	0.9039	0.128	374.0	1.808	424.2	1.186	13.10		980.1
1.4	0.9039	0.179	374.0	1.808	424.2	1.815	17.55		2067.3
1.6	0.9039	0.297	374.0	1.808	424.2	2.768	22.29		4585.4
1.0	0.8424	0.200	508.0	1.685	479.7	1.080	8.40	(8.19)	508.0
1.2	0.8424	0.262	508.0	1.685	479.7	1.863	15.97		1810.9
1.4	0.8424	0.381	508.0	1.685	479.7	2.803	21.11		4291.9
1.6	0.8424	0.695	508.0	1.685	479.7	4.415	26.64		10866.9
1.0	0.7980	0.300	707.0	1.596	524.2	1.498	9.79	(9.54)	707.0
1.2	0.7980	0.400	707.0	1.596	524.2	2.441	17.93		2771.9
1.4	0.7980	0.602	707.0	1.596	524.2	3.661	23.37		6912.0
1.6	0.7980	1.209	707.0	1.596	524.2	5.991	29.52		19416.1
1.0	0.7636	0.400	968.0	1.527	561.6	1.871	11.22	(10.94)	968.0
1.2	0.7636	0.542	968.0	1.527	561.6	2.959	19.46		3858.1
1.4	0.7636	0.840	968.0	1.527	561.6	4.448	25.09		9927.5
1.6	0.7636	1.867	968.0	1.527	561.6	7.602	31.84		30836.7
1.0	0.7358	0.500	1268.0	1.472	593.7	2.211	12.48	(12.24)	1268.0
1.2	0.7358	0.687	1268.0	1.472	593.7	3.435	20.71		5046.4
1.4	0.7358	1.096	1268.0	1.472	593.7	5.190	26.49		13325.4
1.6	0.7358	2.709	1268.0	1.472	593.7	9.308	33.87		45990.3
1.0	0.6839	0.750	2290.0	1.368	658.8	2.962	15.36	(14.97)	2290.0
1.2	0.6839	1.060	2290.0	1.368	658.6	4.500	23.19		8521.4
1.4	0.6839	1.807	2290.0	1.368	658.6	6.920	29.24		23532.6
1.6	0.6839	6.113	2290.0	1.368	658.6	14.397	38.44		110110.2
1.0	0.6472	1.000	3540.0	1.294	708.8	3.613	17.51	(17.06)	3540.0
1.2	0.6472	1.447	3540.0	1.294	708.8	5.441	25.04		12517.7
1.4	0.6472	2.618	3540.0	1.294	708.8	8.541	31.34		36022.4
1.6	0.6472	13.712	3540.0	1.294	708.8	21.989	43.08		258717.9
1.0	0.6244	1.200	4684.0	1.249	741.8	4.084	18.91	(18.42)	4684.0
1.2	0.6244	1.766	4684.0	1.249	741.8	6.133	26.24		18027.5
1.4	0.6244	3.339	4684.0	1.249	741.8	9.790	32.72		47591.0
1.6	0.6244	30.707	4684.0	1.249	741.8	33.288	47.79		596573.5

[a] Values in parentheses were calculated by McQueen et al. (1970).

BARIUM

Because of the large compressions achieved for this metal, the Grüneisen parameter uncertainties are large. This and the uncertainty in the thermochemical data indicate that the present calculation should be accepted only on a very tentative basis. Taken at face value, the calculations indicate that 4- to 5-km/sec aluminum flyer plates will partially vaporize this metal for both m = 1.0 and m = 1.2 distentions. Iron and tungsten flyer plates should achieve vaporizations of approximately 50% at these speeds for distentions of m = 1.2 or greater.

THORIUM

The uncertainty in the boiling point of this metal gives rise to considerable uncertainty about the entropy required for incipient vaporization. For a 5-km/sec aluminum flyer plate the optimum distention

Table 3. Shock-wave parameters and thermodynamic states for pure iron.

Distention ratio (V_{00}/V_0)	Compression (V/V_0)	Shock pressure (Mbar)	Principal Hugoniot shock temp (°K)	Grüneisen ratio	Debye temp (°K)	Shock particle velocity (km/sec)	Entropy[a] (cal mol-°K)		Porous Hugoniot shock temp (°K)
1.0	0.8803	0.200	416.0	1.488	214.2	0.552	11.92	(11.95)	416.0
1.2	0.8803	0.246	416.0	1.488	214.2	1.002	18.27		1208.4
1.4	0.8803	0.321	416.0	1.488	214.2	1.457	22.55		2478.4
1.6	0.8803	0.459	416.0	1.488	214.2	2.051	26.54		4843.8
1.8	0.8803	0.807	416.0	1.488	214.2	3.074	31.32		10796.8
1.0	0.8215	0.400	657.0	1.388	236.6	0.954	14.03	(14.06)	657.0
1.2	0.8215	0.499	657.0	1.388	236.6	1.552	21.61		2345.1
1.4	0.8215	0.664	657.0	1.388	236.6	2.213	26.29		5149.5
1.6	0.8215	0.993	657.0	1.388	236.6	3.138	30.67		10724.2
1.8	0.8215	1.961	657.0	1.388	236.6	4.945	36.21		27179.6
1.0	0.7829	0.600	1007.0	1.323	252.6	1.288	16.17	(16.21)	1007.0
1.2	0.7829	0.757	1007.0	1.323	252.6	2.005	23.86		3659.4
1.4	0.7829	1.024	1007.0	1.323	252.6	2.837	28.66		8185.3
1.6	0.7829	1.583	1007.0	1.323	252.6	4.059	33.24		17652.9
1.8	0.7829	3.486	1007.0	1.323	252.6	6.720	39.43		49888.2
1.0	0.7544	0.800	1444.0	1.275	265.0	1.582	18.03	(18.06)	1444.0
1.2	0.7544	1.017	1444.0	1.275	265.0	2.403	25.56		5113.3
1.4	0.7544	1.395	1444.0	1.275	265.0	3.387	30.40		11511.6
1.6	0.7544	2.221	1444.0	1.275	265.0	4.891	35.13		25485.5
1.8	0.7544	5.443	1444.0	1.275	265.0	8.515	41.95		80012.3
1.0	0.7317	1.200	2523.0	1.237	275.4	2.025	21.12	(20.97)	2523.0
1.2	0.7317	1.536	2523.0	1.237	275.4	3.027	28.14		8194.6
1.4	0.7317	2.132	2523.0	1.237	275.4	4.260	32.92		18270.2
1.6	0.7317	3.485	2523.0	1.237	275.4	6.208	37.75		41134.7
1.8	0.7317	9.538	2523.0	1.237	275.4	11.393	45.20		143435.6
1.0	0.6827	1.600	3812.0	1.154	299.2	2.543	23.09	(23.12)	3812.0
1.2	0.6827	2.080	3812.0	1.154	299.2	3.703	29.89		11927.0
1.4	0.6827	2.973	3812.0	1.154	299.2	5.212	34.76		27005.8
1.6	0.6827	5.207	3812.0	1.154	299.2	7.801	39.97		64747.9
1.8	0.6827	20.955	3812.0	1.154	299.2	17.270	49.69		330765.3
1.0	0.6588	2.000	5264.0	1.113	311.5	2.948	24.78	(24.80)	5264.0
1.2	0.6588	2.623	5264.0	1.113	311.5	4.252	31.32		15783.1
1.4	0.6588	3.809	5264.0	1.113	311.5	5.997	36.30		35816.6
1.6	0.6588	6.954	5264.0	1.113	311.5	9.131	41.62		88931.4
1.8	0.6588	39.884	5264.0	1.113	311.5	24.079	53.42		645103.1
1.0	0.6388	2.400	6846.0	1.080	322.2	3.323	25.14	(26.16)	6846.0
1.2	0.6388	3.171	6846.0	1.080	322.2	4.762	32.49		19873.1
1.4	0.6388	4.674	6846.0	1.080	322.2	6.732	37.39		45241.4
1.6	0.6388	8.880	6846.0	1.080	322.2	10.427	43.01		116270.3
1.8	0.6388	88.753	6846.0	1.080	322.2	36.234	58.11		1465124.6
1.0	0.6256	2.700	8107.0	1.057	329.5	3.589	27.01	(27.04)	8107.0
1.2	0.6256	3.587	8107.0	1.057	329.5	5.123	33.25		23079.4
1.4	0.6256	5.340	8107.0	1.057	329.5	7.258	38.17		52693.6
1.6	0.6256	10.450	8107.0	1.057	329.5	11.389	43.94		138976.6

[a]Values in parentheses were calculated by McQueen et al. (1970) for 1018 alloy.

is approximately 1.8 (see Fig. 6(a), but this probably will not induce even partial vaporization. For 4- to 5-km/sec iron flyer plates the optimum distention is 1.8 to 2.0, which will induce partial vaporization (see Fig. 6(b)). Tungsten plates fired at samples with distentions greater than 2.0 will induce maximum, but probably only 5% vaporization (see Fig. 6(c)).

URANIUM

The Mie-Grüneisen equation sharply limits the present calculations to shocks in a regime of lower entropy than required for partial vaporization. This metal is a good candidate for Mach-stem vaporization, which is discussed in the following sections. Extrapolating the results of Fig. 7(c) suggests that a 4- or 5-km/sec tungsten plate fired at a 1.8 distention target may induce some partial vaporization. This, however, is a very tentative speculation.

LITHIUM

As evident from Fig. 8, lithium is surprisingly difficult to vaporize with a plane-wave system. For the range of distention up to a value of 1.6, no flyer plate is capable of shocking the material to even induce partial vaporization; therefore lithium is another good candidate for Mach-stem vaporization.

STRONTIUM

Substantial quantities of strontium vapor can be produced by shocking either initially solid or distention 1.2 samples with 4- or 5-km/sec tungsten or iron flyer plates (see Figs. 9(a) and 9(b)). As for the other compressible metals, the Mie-Grüneisen theory is not usable for greater porosities. Although the limited range explored suggests rather high porosities, m = 1.6 may be optimum for vapor production.

Table 4. Shock-wave parameters and thermodynamic states for barium.

Distention ratio (V_{00}/V_0)	Compression (V/V_0)	Shock pressure (Mbar)	Principal Hugoniot shock temp (°K)	Grüneisen ratio	Debye temp (°K)	Shock particle velocity (km/sec)	Entropy (cal/mol-°K)	Porous Hugoniot shock temp (°K)
1.0	0.6650	0.0510	1035.0	1.343	172.5	0.698	18.60	1035.0
1.2	0.6650	0.0734	1035.0	1.343	172.5	1.058	24.49	2779.1
1.0	0.5810	0.1020	2329.0	1.270	187.3	1.103	22.95	2329.0
1.2	0.5810	0.1709	2329.0	1.270	187.3	1.736	29.74	7280.4
1.0	0.4720	0.3030	9457.0	1.146	201.5	2.135	30.86	9457.0
1.2	0.4720	0.9360	9457.0	1.146	201.5	4.406	40.83	50373.1
1.0	0.4320	0.5040	17918.0	1.093	204.7	2.856	34.58	17918.0
1.2	0.4320	4.9869	17918.0	1.093	204.7		51.29	295978.1

Table 5. Shock-wave parameters and thermodynamic states for thorium.

Distention ratio (V_{00}/V_0)	Compression (V/V_0)	Shock pressure (Mbar)	Principal Hugoniot shock temp (°K)	Grüneisen ratio	Debye temp (°K)	Shock particle velocity (km/sec)	Entropy (cal/mol-°K)	Porous Hugoniot shock temp (°K)
1.0	0.7950	0.200	667.0	1.000	208.7	0.592	14.86	667.0
1.2	0.7950	0.234	667.0	1.000	208.7	0.900	23.44	2814.8
1.4	0.7950	0.281	667.0	1.000	208.7	1.207	27.78	5835.1
1.6	0.7950	0.353	667.0	1.000	208.7	1.559	31.22	10394.2
1.8	0.7950	0.474	667.0	1.000	208.7	2.016	34.52	18070.6
2.0	0.7950	0.718	667.0	1.000	208.7	2.724	38.24	33722.5
1.0	0.7070	0.400	1577.0	0.890	220.6	1.002	19.64	1577.0
1.2	0.7070	0.473	1577.0	0.890	220.6	1.413	27.81	6204.7
1.4	0.7070	0.579	1577.0	0.890	220.6	1.853	32.17	12899.0
1.6	0.7070	0.745	1577.0	0.890	220.6	2.387	35.73	23441.8
1.8	0.7070	1.045	1577.0	0.890	220.6	3.128	39.27	42480.9
2.0	0.7070	1.752	1577.0	0.890	220.6	4.405	43.56	87302.6
1.0	0.6520	0.600	2708.0	0.820	226.1	1.337	22.72	2708.0
1.2	0.6520	0.715	2708.0	0.820	226.1	1.832	30.51	10006.8
1.4	0.6520	0.885	2708.0	0.820	226.1	2.381	34.86	20771.9
1.6	0.6520	1.161	2708.0	0.820	226.1	3.069	38.50	38241.7
1.8	0.6520	1.685	2708.0	0.820	226.1	4.070	42.23	71512.4
2.0	0.6520	3.077	2708.0	0.820	226.1	5.959	47.02	159720.8
1.0	0.6140	0.800	3659.0	0.770	228.8	1.626	24.45	3659.0
1.2	0.6140	0.958	3659.0	0.770	228.8	2.193	32.33	13739.7
1.4	0.7140	1.196	3659.0	0.770	228.8	2.837	36.74	28805.9
1.6	0.6140	1.588	3659.0	0.770	228.8	3.662	40.46	53770.9
1.8	0.6140	2.366	3659.0	0.770	228.8	4.801	44.34	103162.9
2.0	0.6140	4.631	3659.0	0.770	228.8	7.413	49.55	247173.2
1.0	0.5850	1.000	5091.0	0.740	231.1	1.885	26.36	5091.0
1.2	0.5850	1.207	5091.0	0.740	231.1	2.521	33.92	18133.8
1.4	0.5850	1.522	5091.0	0.740	231.1	3.259	38.33	37986.9
1.6	0.5850	2.060	5091.0	0.740	231.1	4.231	42.13	71868.1
1.8	0.5850	3.185	5091.0	0.740	231.1	5.756	46.22	142789.7
2.0	0.5850	7.021	5091.0	0.740	231.1	9.223	52.12	284434.7
1.0	0.5620	1.200	7239.0	0.710	232.0	2.121	28.43	7239.0
1.2	0.5620	1.454	7239.0	0.710	232.0	2.818	35.38	23256.8
1.4	0.5620	1.844	7239.0	0.710	232.0	3.638	39.68	47873.5
1.6	0.5620	2.521	7239.0	0.710	232.0	4.733	43.48	90554.1
1.8	0.5620	3.982	7239.0	0.710	232.0	6.496	47.66	182705.5
2.0	0.5620	9.470	7239.0	0.710	232.0	10.798	54.00	528892.8
1.0	0.5440	1.400	9666.0	0.680	231.8	2.338	30.16	9666.0
1.2	0.5440	1.697	9666.0	0.680	231.8	3.087	36.62	28574.0
1.4	0.5440	2.153	9666.0	0.680	231.8	3.972	40.80	57647.6
1.6	0.5440	2.944	9666.0	0.680	231.8	5.159	44.5	108098.6
1.8	0.5440	4.656	9666.0	0.680	231.8	7.076	48.70	217213.4
2.0	0.5440	11.122	9666.0	0.680	231.8	11.775	55.04	629424.1
1.0	0.5350	1.500	10980.0	0.670	232.1	2.444	30.91	10980.0
1.2	0.5350	1.822	10980.0	0.670	232.1	3.221	37.18	31460.5
1.4	0.5350	2.320	10980.0	0.670	232.1	4.145	41.33	63132.3
1.6	0.5350	3.192	10980.0	0.670	232.1	5.395	45.09	118616.8
1.8	0.5350	5.114	10980.0	0.670	232.1	7.442	49.31	240946.7
2.0	0.5350	12.862	10980.0	0.670	232.1	12.702	55.95	733928.4

Table 6. Shock-wave parameters and thermodynamic states for pure uranium.

Distention ratio (V_{00}/V_0)	Compression (V/V_0)	Shock pressure (Mbar)	Principal Hugoniot shock temp (°K)	Grüneisen ratio	Debye temp (°K)	Shock particle velocity (km/sec)	Entropy[a] (cal/mol-°K)		Porous Hugoniot shock temp (°K)
1.0	0.8872	0.200	436.0	1.801	345.8	0.344	9.40	(10.81)	436.0
1.2	0.8872	0.259	436.0	1.801	345.8	0.653	18.32		1950.8
1.4	0.8872	0.369	436.0	1.801	345.8	0.997	23.62		4748.2
1.0	0.8241	0.400	759.0	1.673	393.0	0.608	11.88	(13.65)	759.0
1.2	0.8241	0.531	759.0	1.673	393.0	1.024	21.85		4044.3
1.4	0.8241	0.791	759.0	1.673	393.0	1.546	27.58		10540.1
1.0	0.8159	0.600	1267.0	1.656	399.6	0.761	14.81	(16.50)	1267.0
1.2	0.8159	0.800	1267.0	1.656	399.6	1.270	24.29		6317.8
1.4	0.8159	1.198	1267.0	1.656	399.6	1.917	29.98		16105.8
1.0	0.7245	1.000	2737.0	1.471	481.1	1.203	18.29	(21.00)	2737.0
1.2	0.7245	1.392	2737.0	1.471	481.1	1.864	27.31		12443.4
1.4	0.7245	2.291	2737.0	1.471	481.1	2.851	33.42		34885.3
1.0	0.6795	1.500	5219.0	1.379	527.1	1.589	21.59	(24.75)	5219.0
1.2	0.6795	2.146	5219.0	1.379	527.1	2.421	29.93		21168.8
1.4	0.6795	3.767	5219.0	1.379	527.1	3.774	36.26		61218.8
1.0	0.6485	2.000	8225.0	1.316	561.3	1.921	23.93	(27.43)	8225.0
1.2	0.6485	2.922	8225.0	1.316	561.3	2.909	31.83		31002.0
1.4	0.6485	5.423	8225.0	1.316	561.3	4.625	38.36		92759.6
1.0	0.6254	2.500	11622.0	1.270	588.3	2.217	25.71	(29.47)	11622.0
1.2	0.6254	3.718	11622.0	1.270	588.3	3.349	33.32		41689.6
1.4	0.6254	7.248	11622.0	1.270	586.3	5.429	40.04		128859.4
1.0	0.6072	3.000	15327.0	1.233	610.4	2.487	27.14	(31.12)	15327.0
1.2	0.6072	4.529	15327.0	1.233	610.4	3.754	34.54		53078.2
1.4	0.6072	9.236	15327.0	1.233	610.4	6.200	41.45		169304.5
1.0	0.5924	3.500	19282.0	1.203	629.0	2.737	28.32	(32.49)	19282.0
1.2	0.5924	5.354	19282.0	1.203	629.0	4.132	35.57		65048.9
1.4	0.5924	11.382	19282.0	1.203	629.0	6.948	42.68		213881.4

[a] Values in parentheses were calculated by McQueen et al. (1970) for 97/3 uranium/molybdenum alloy.

Table 7. Shock-wave parameters and thermodynamic states for lithium.

Distention ratio (V_{00}/V_0)	Compression (V/V_0)	Shock pressure (Mbar)	Principal Hugoniot shock temp (°K)	Grüneisen ratio	Debye temp (°K)	Shock particle velocity (km/sec)	Entropy (cal/mol-°K)	Porous Hugoniot shock temp (°K)
1.0	0.7510	0.0540	498.0	1.023	477.3	1.593	8.31	496.0
1.2	0.7510	0.0646	498.0	1.023	477.3	2.339	12.00	925.4
1.4	0.7510	0.0804	498.0	1.023	477.3	3.137	15.12	1561.4
1.6	0.7510	0.1063	498.0	1.023	477.3	4.127	18.18	2608.4
1.0	0.6610	0.1020	777.0	0.958	512.0	2.554	10.47	777.0
1.2	0.6610	0.1263	777.0	0.958	512.0	3.583	15.05	1675.2
1.4	0.6610	0.1657	777.0	0.958	512.0	4.806	18.78	3133.9
1.6	0.6610	0.2408	777.0	0.958	512.0	6.531	22.57	5915.8
1.0	0.5880	0.1670	1287.0	0.899	535.9	3.603	13.17	1287.0
1.2	0.5880	0.2150	1287.0	0.899	535.9	4.982	18.11	2948.7
1.4	0.5880	0.3016	1287.0	0.899	535.9	6.798	22.29	5950.0
1.6	0.5880	0.5054	1287.0	0.899	535.9	9.823	26.95	13005.6
1.0	0.5280	0.2530	2133.0	0.846	551.6	4.747	15.99	2133.0
1.2	0.5280	0.3408	2133.0	0.846	551.6	6.574	21.09	5020.6
1.4	0.5280	0.5220	2133.0	0.846	551.6	9.267	25.75	10978.2
1.6	0.5280	1.1144	2133.0	0.846	551.6		31.83	30458.2

Table 8. Shock-wave parameters and thermodynamic states for pure aluminum.

Distention ratio (V_{00}/V_0)	Compression (V/V_0)	Shock pressure (Mbar)	Principal Hugoniot shock temp (°K)	Grüneisen ratio	Debye temp (°K)	Shock particle velocity (km/sec)	Entropy (cal/mol-°K)	Porous Hugoniot shock temp (°K)
1.0	0.7150	0.059	738.3	1.138	203.3	0.805	15.62	738.3
1.2	0.7150	0.074	738.3	1.138	203.3	1.178	21.68	2043.3
1.0	0.6210	0.100	1563.0	1.060	219.7	1.206	19.62	1563.0
1.2	0.6210	0.133	1563.0	1.060	219.7	1.724	25.56	4233.9
1.0	0.5665	0.149	2674.0	1.009	227.7	1.579	22.61	2674.0
1.2	0.5665	0.210	2674.0	1.009	227.7	2.265	28.60	7312.4
1.0	0.5276	0.202	4089.0	0.971	232.6	1.917	34.98	4069.0
1.2	0.5276	0.300	4089.0	0.971	232.6	2.785	31.04	11244.3
1.0	0.5016	0.250	5473.0	0.945	235.4	2.180	26.68	5473.0
1.2	0.5016	0.387	5473.0	0.945	235.4	3.228	32.82	15355.2
1.0	0.4808	0.298	7005.0	0.924	237.5	2.442	28.09	7005.0
1.2	0.4808	0.484	7005.0	0.924	237.5	3.661	34.37	20073.0
1.0	0.4471	0.406	10679.0	0.889	240.3	2.939	30.54	10679.0
1.2	0.4471	0.726	10679.0	0.889	240.3	4.589	37.17	32505.0
1.0	0.4133	0.568	16787.0	0.852	242.3	3.583	33.18	16787.0
1.2	0.4133	1.188	16787.0	0.852	242.3	5.999	40.51	57456.1

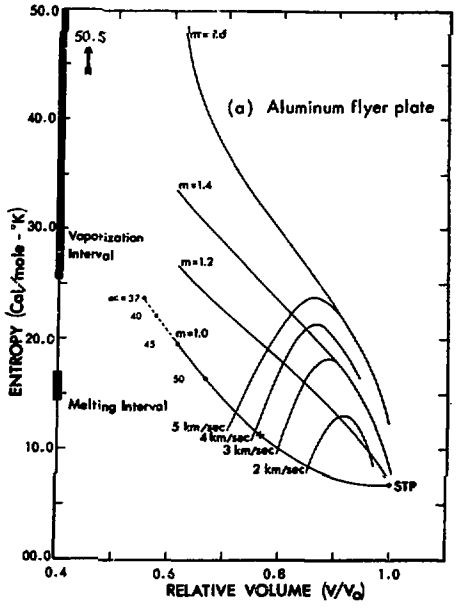

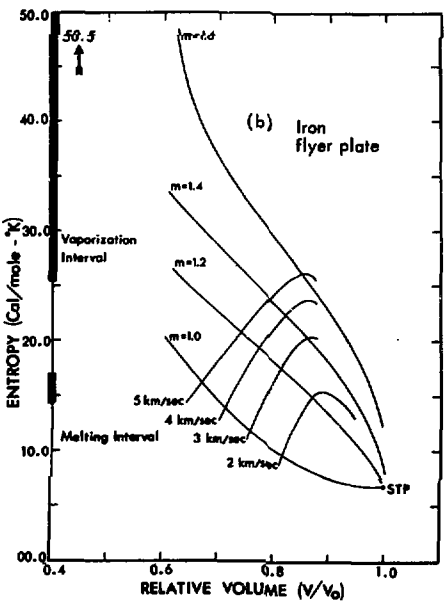

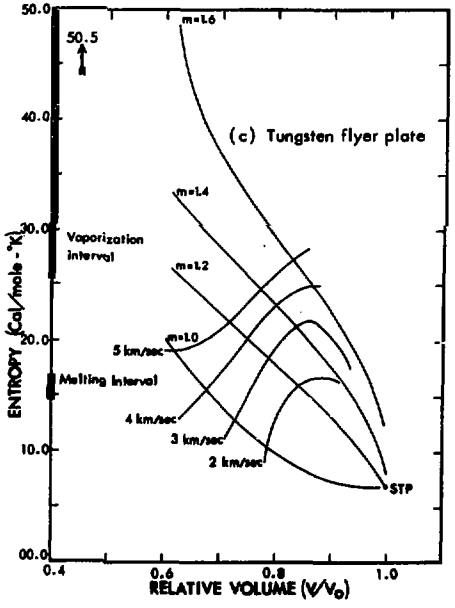

Fig. 3. Hugoniot curves for aluminum showing various initial distention ratios, m, on the entropy-relative volume plane. The second set of curves represents the loci of states attainable at different flyer plate speeds. The points indicated by a solid dot (●) represent the states behind the Mach stems formed by the collision of two shock waves (indicated by +) at the indicated angles of incidence.

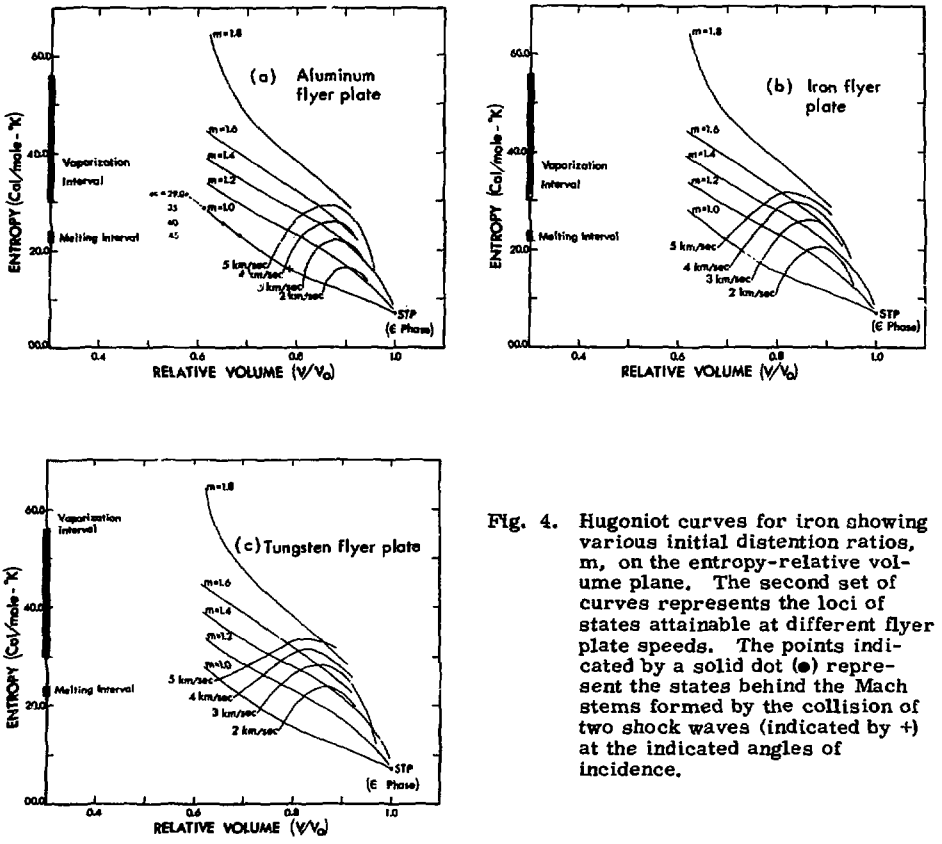

Fig. 4. Hugoniot curves for iron showing various initial distention ratios, m, on the entropy-relative volume plane. The second set of curves represents the loci of states attainable at different flyer plate speeds. The points indicated by a solid dot (●) represent the states behind the Mach stems formed by the collision of two shock waves (indicated by +) at the indicated angles of incidence.

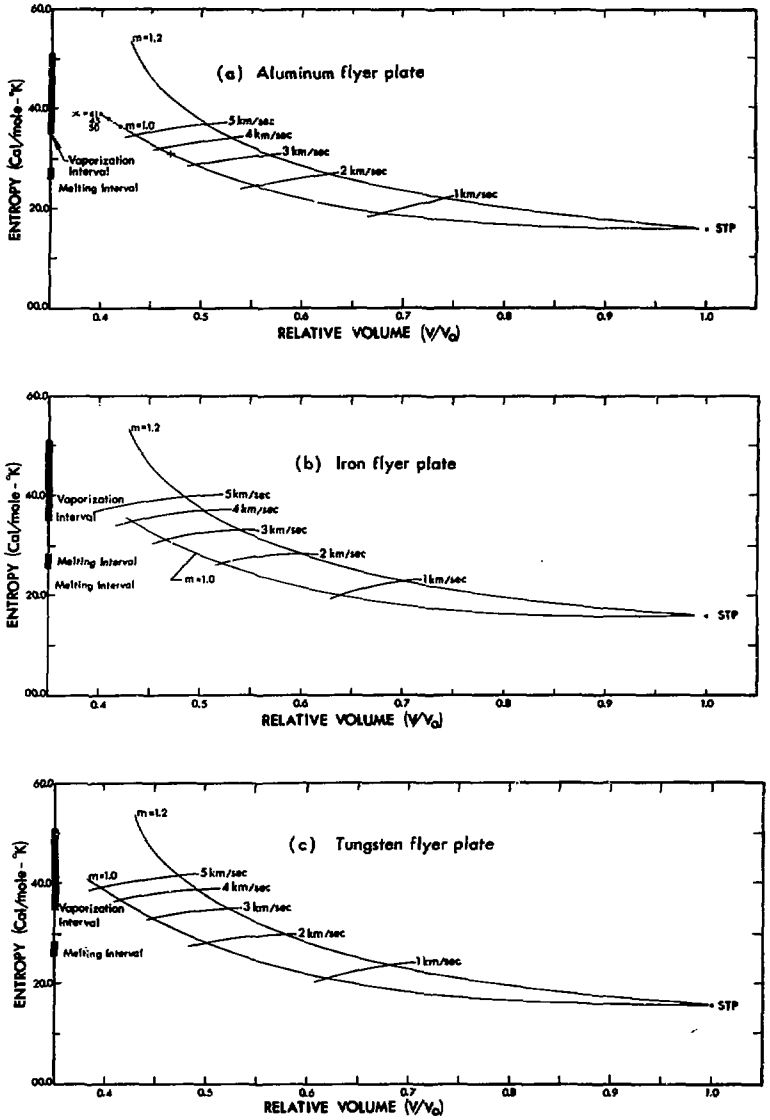

Fig. 5. Hugoniot curves for barium showing various initial distention ratios, m, on the entropy-relative volume plane. The second set of curves represents the loci of states attainable at different flyer plate speeds. The points indicated by a solid dot (●) represent the states behind the Mach stems formed by the collision of two shock waves (indicated by +) at the indicated angles of incidence.

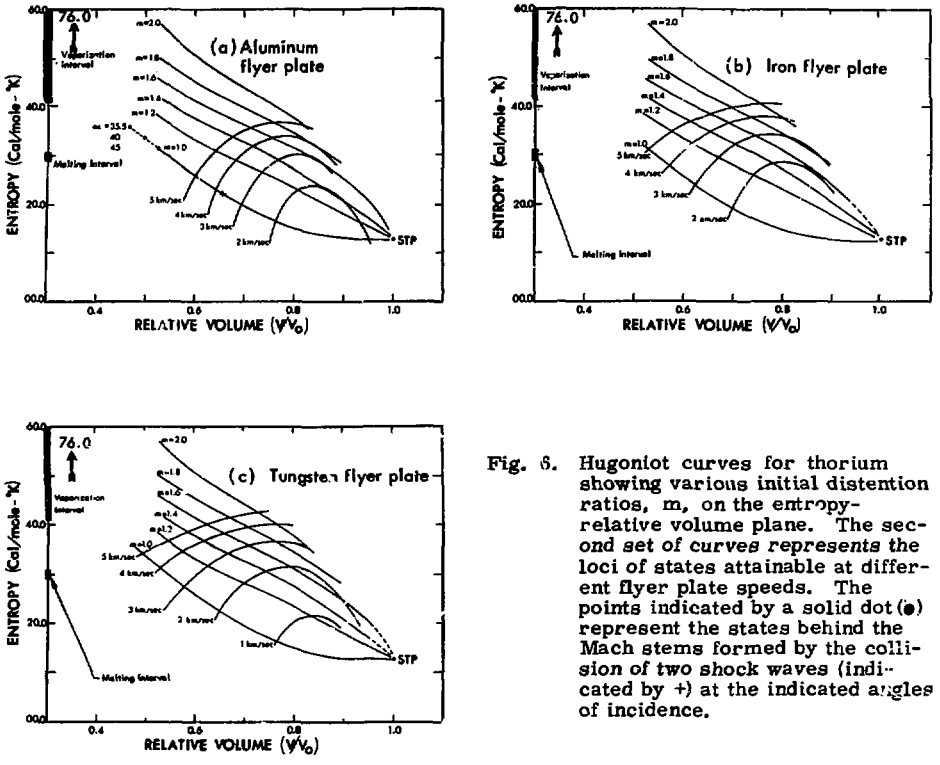

Fig. 6. Hugoniot curves for thorium showing various initial distention ratios, m, on the entropy-relative volume plane. The second set of curves represents the loci of states attainable at different flyer plate speeds. The points indicated by a solid dot (●) represent the states behind the Mach stems formed by the collision of two shock waves (indicated by +) at the indicated angles of incidence.

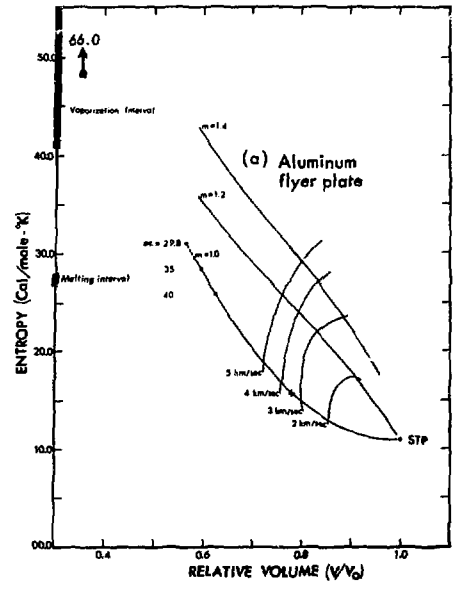

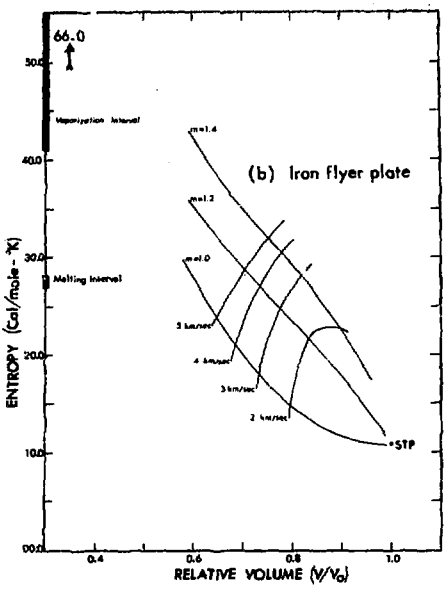

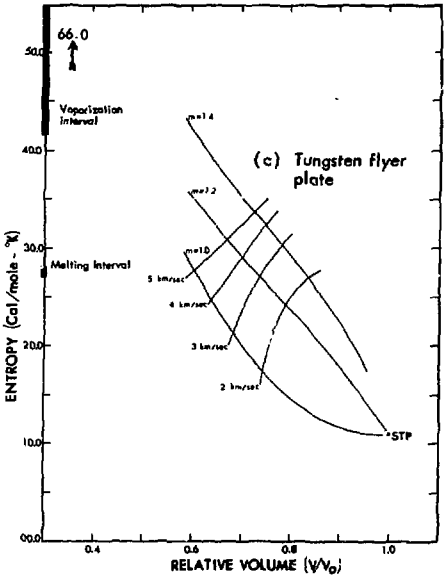

Fig. 7. Hugoniot curves for uranium showing various initial distention ratios, m, on the entropy-relative volume plane. The second set of curves represents the loci of states attainable at different flyer plate speeds. The points indicated by a solid dot (●) represent the states behind the Mach stems formed by the collision of two shock waves (indicated by +) at the indicated angles of incidence.

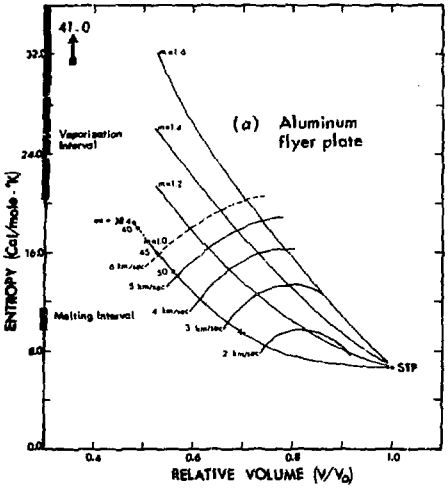

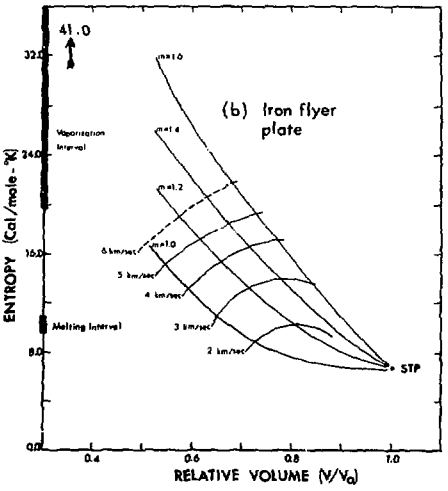

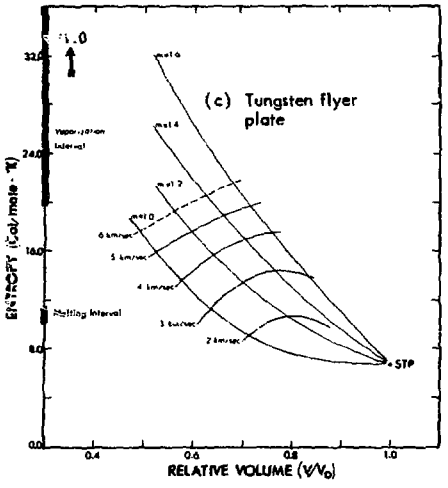

Fig. 8. Hugoniot curves for lithium showing various initial distention ratios, m, on the entropy-relative volume plane. The second set of curves represents the loci of states attainable at different flyer plate speeds. The points indicated by a solid dot (●) represent the states behind the Mach stems formed by the collision of two shock waves (indicated by +) at the indicated angles of incidence.

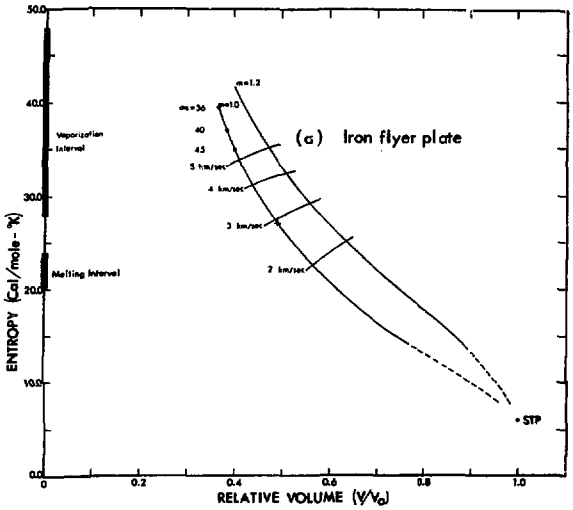

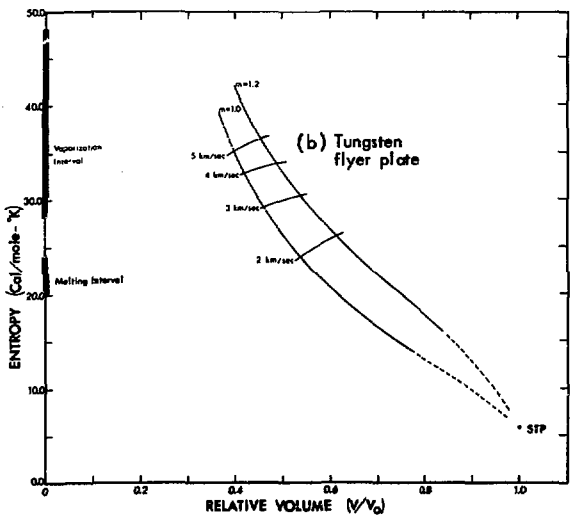

Fig. 9. Hugoniot curves for strontium showing various initial distention ratios, m, on the entropy-relative volume plane. The second set of curves represents the loci of states attainable at different flyer plate speeds. The points indicated by a solid dot (●) represent the states behind the Mach stems formed by the collision of two shock waves (indicated by +) at the indicated angles of incidence.

Mach Stems

In order to calculate the entropies that may be induced, particularly in lithium and uranium, upon propagation of Mach stems, we have initially investigated the criteria for introducing this type of flow in all the metals of interest. For the present we have considered these metals only at the single crystal density.

Upon the collision of two shocks at a slightly oblique angle, the pressure behind the reflected shock will increase slightly as the incidence angle, α, increases. At a certain critical angle, α_{cr}, regular reflection will no longer occur, and a Mach stem will be formed similar to that shown in Fig. 10(b). With the formation of a Mach stem, the pressure produced will increase discontinuously to a new high value. Upon further increase in α, this pressure will rapidly decrease until at $\alpha = 90$ it will reach the value of the original plane shock wave.

The theory of oblique shock waves for gaseous media is fully described in a classical text of Courant and Friedrichs,[17] and the description of irregular reflection in solid bodies was carried out by Al'tshuler and his co-workers.[18] The application of Mach stems to the study of properties of materials under extremely high pressures has been discussed by Leygonie and Bergon[19] and more recently by de Beaumont and Leygonie.[20] In the latter paper the authors describe producing Mach stems by a convergent conical shock wave in copper and using the central portion of the Mach stem to impact as a strong plane wave upon a small pellet of uranium sample. This is a candidate, but unexplored, configuration that might be used in proposed experiments in this country.

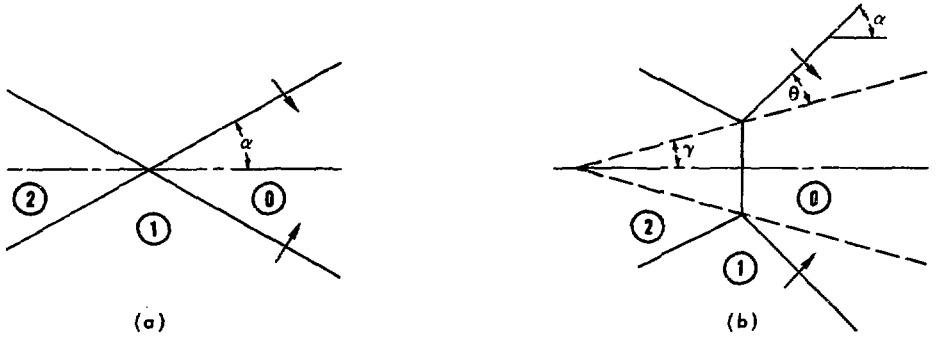

Fig. 10. Oblique intersection of shock waves: (a) regular Mach stem; (b) irregular Mach stem.

Oblique Shock Polars

The present analysis is carried out graphically. The method was initially developed for the solution of problems involving the interaction of oblique discontinuities in gaseous media[21] and it has also been applied to liquid explosives.[22] For solid bodies a similar technique was developed by Laharrague et al.[23] for problems involving shock-wave refraction from a boundary between two different materials.

In contrast to the other polar techniques known in the literature, the vector polar method uses a logarithmic scale for the pressure ratio, which permits not only a more compact set of polars but also graphical addition of pressure ratios across various components of the wave system.

The basic theory describing the flow across an oblique discontinuity in a solid material is illustrated in Fig. 11 and is governed by the following set of equations:

$$\rho_0 u_s = \rho_1 (u_s - u_p), \tag{14}$$

$$p_1 - p_0 = \rho_0 u_s u_p, \tag{15}$$

$$u_s = a_0 + b_0 u_p, \tag{16}$$

$$u_s = w \sin \theta, \tag{17}$$

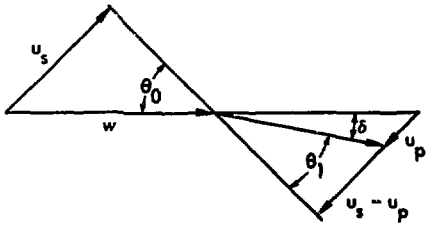

Fig. 11. Geometrical diagram of the flow across an oblique shock wave.

and

$$\delta = \theta_0 - \theta_1. \tag{18}$$

Here p, ρ, u_s and u_p denote the usual pressure, density, normal shock velocity, and normal particle velocity; a and b represent the two constants in the linear $u_s - u_p$ relationship in solids (McQueen et al.[6]); w is the oblique shock velocity, while θ and δ denote the oblique angle of approach and the angle by which the flow was deflected after going through the oblique shock discontinuity. The subscripts 0 and 1 indicate the undisturbed and shocked states, respectively.

These equations were found to be easier to manipulate if they are cast in a nondimensional form. This is done by using $p_0 v_0$ as a normalizing parameter where v_0 is the initial specific volume; i.e., $v_0 = 1/\rho_0$. With $\nu = v/v_0$ and $P = p/p_0$, the first four equations are written as follows:

$$U_p = (1 - \nu) U_s, \tag{14a}$$

$$(P - 1) = U_s U_p, \tag{15a}$$

$$U_s = A_0 + b U_p, \tag{16a}$$

and

$$U_s = W_0 \sin \theta. \tag{17a}$$

In contrast to the dimensional form, all nondimensional quantities are represented as capital letters.

Introducing a new parameter,

$$\Gamma_k = \frac{a_k^2}{p_k v_k},$$

one can derive the Mach number, which is a well-known parameter in gas dynamics:

$$M_k^2 = \frac{w_k^2}{a_k^2} = \frac{W_k^2}{\Gamma_k} \qquad k = i,j,$$

where i and j indicate conditions before and after the wave. In solid materials Mach number has little meaning, since it is normalized by a bulk sound velocity of the medium; nevertheless it is a very useful quantity for this analysis.

With these parameters one can derive the following equations:

$$(P - 1) = \frac{\Gamma_i(1 - \nu)}{[1 - b(1 - \nu)]^2}, \tag{19}$$

$$(P - 1) = (1 - \nu)\Gamma_i M_i^2 \sin^2 \theta, \tag{20}$$

$$\tan \delta = \frac{(P - 1)\cot \theta}{\Gamma_i M_i^2 - (P - 1)}, \tag{21}$$

and

$$M_j^2 = \frac{\Gamma_i M_i^2 - (P - 1)(1 + \nu)}{\Gamma_j P \nu}. \tag{22}$$

The solutions to these equations are plotted in the form of polars on the P - δ, θ - δ, and P - M_j planes as shown in

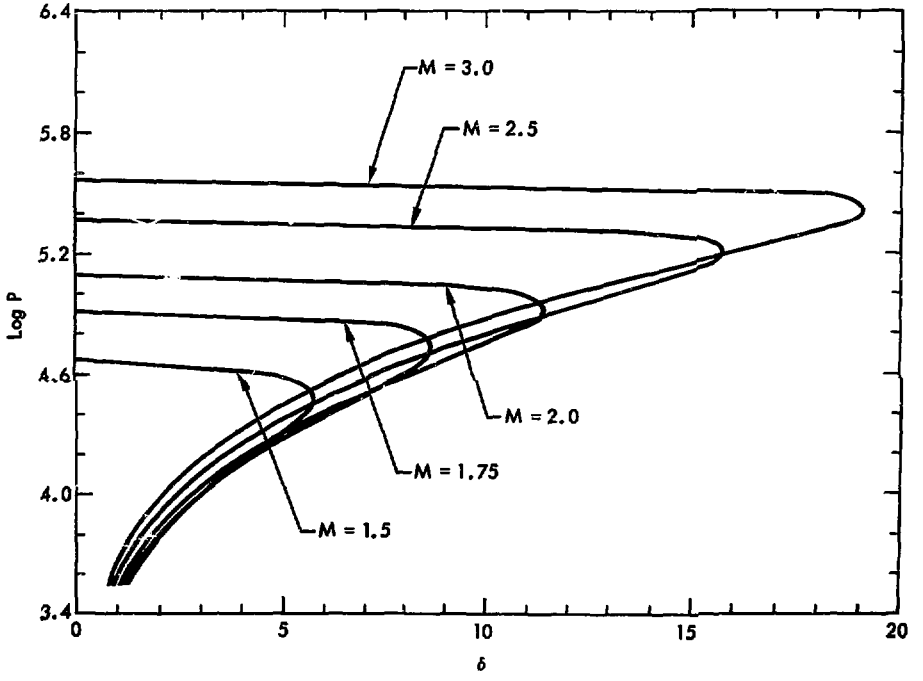

Fig. 12. Oblique shock polars for strontium in the pressure ratio-deflection angle plane.

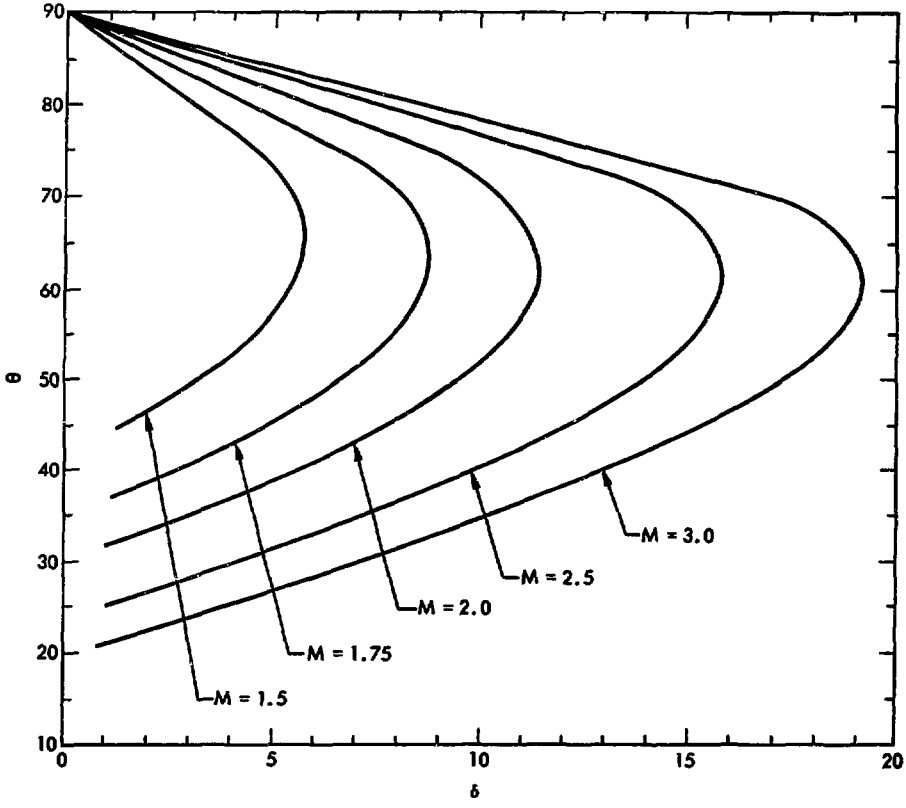

Fig. 13. Oblique shock polars for strontium in the incident angle-deflection angle plane.

Figs. 12, 13, and 14, respectively. The incident Mach number of the wave was taken as an independent parameter, and the plot shows polars for several values of M_2. For a solution of a problem, all three planes are equally important and must be used simultaneously—even though only one P - δ plane is considered to be the main solution plane since pressure and deflection angle represent the two most interesting parameters of the flow.

The reflected shock waves that propagate into a precompressed region are calculated in the same manner using the same set of four Eqs. (19)-(22), the only difference being that M_1 and Γ_i correspond to the new initial conditions of the state into which the wave propagates.

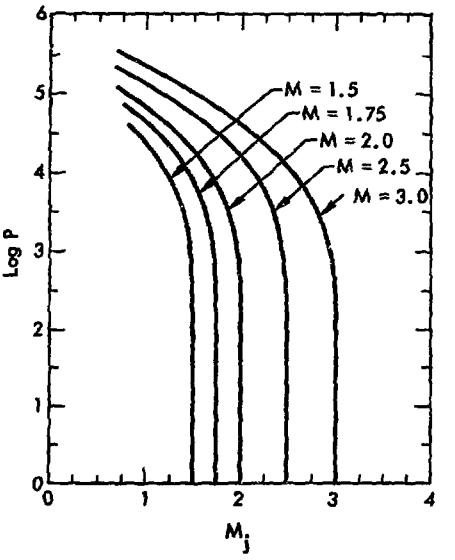

Fig. 14. Oblique shock polars for strontium in the pressure ratio-downstream Mach number plane.

Critical Angle

Solving for the critical angle at which regular reflection becomes irregular, one first assumes the strength of the shock wave that is to interact with its identical counterpart at an oblique angle α. The same wave inclined at different angles will have the same Γ_j, but different M_i, and therefore different M_j. Reflected shock polars are computed and plotted on the P - δ plane with their origin placed at proper initial states as illustrated in Fig. 15. For example, let us assume two shock waves propagating through strontium at a velocity of 3.18 mm/μsec with a pressure p_1 = 100 kbar. The intersection of the reflected polar with either the ordinate (δ = 0) or the original shock polar ($\delta > 0$) will determine whether reflection is regular or irregular, respectively—i.e., whether the Mach stem has formed during this reflection. As evident from Fig. 15, there is a range of cases where reflected shock intersects both, and this range corresponds to the two-solution region, one of which, the one with the lower pressure, is more likely to occur. When the reflected shock polar becomes tangent to the ordinate, the angle at which this occurs is said to be critical, because further increase of the incident angle will only produce irregular reflection with a Mach stem.

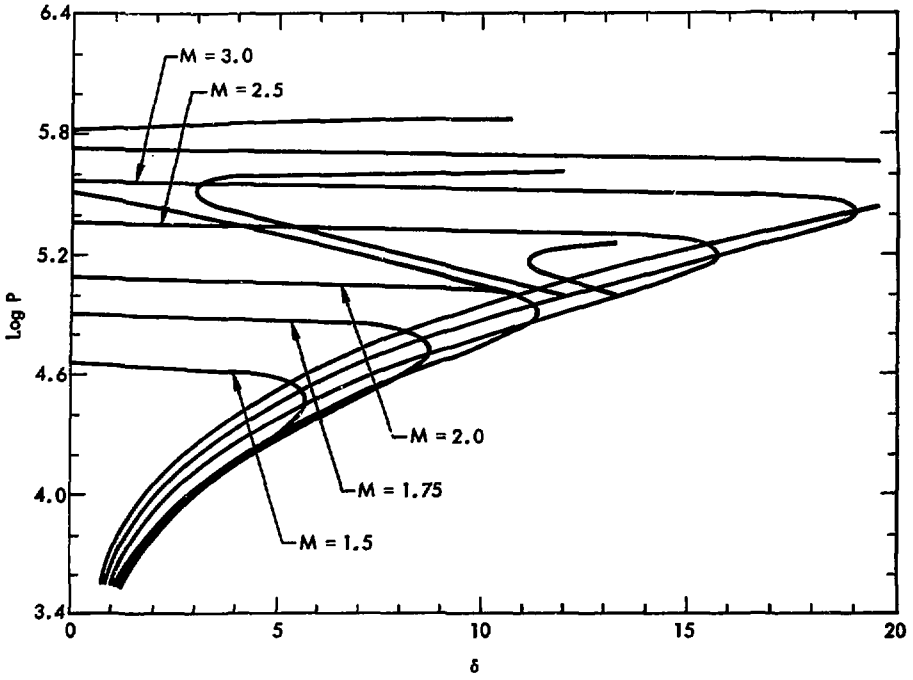

Fig. 15. Oblique shock polars for incident and reflected waves in strontium.

Upon solution for the critical angles, it became evident that there are several ways a transition from a regular reflection to an irregular one can occur. The type of transition depends not only on the material that is used, but also on the initial strength of the interacting shock waves. The three types of solutions are illustrated in Fig. 16, where all three cases show the secondary shock polar to be tangent with the $\delta = 0$ ordinate.

In type I, the entire reflected shock polar lies below the original polar without crossing it at any point. This failure to have a common point between the two polars other than the origin of the reflected one indicates that the case is not merely a simple triple wave intersection, but rather a more complex one involving additional compression along the Mach stem, as illustrated in a qualitative manner in Fig. 16.

Type II is probably the most common type when at the critical angle the reflected polar also crosses the original one at a certain $\delta > 0$. Although in this case the solution calls for a distinct three-wave configuration at the origin of the Mach stem, the flow behind it is not entirely uniform and must adjust itself from a slightly oblique wave at the axis of symmetry.

Type III is special; the Mach stem is already being formed before the critical

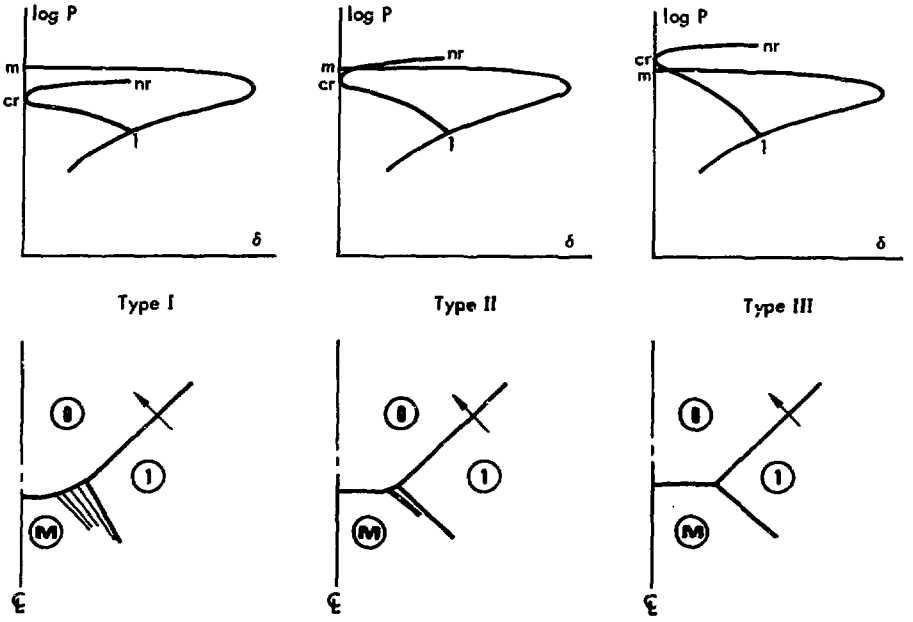

Fig. 16. Three types of Mach configurations of critical angles.

angle criterion has been achieved. In this case it is possible to find an angle at which a perfect Mach stem is formed that is normal to the axis of symmetry over its entire length.

The variation of the critical angle for the metals of interest with initial strength of the shock wave is shown in Fig. 17. The ranges of investigation for various materials are dictated by the relative impedance of the materials and by our ability to attain the necessary pressures with the simple high-explosive techniques described in the first part of this report.

Some of the materials show similar tendencies with an increase in shock pressure in that the critical angle decreases asymptotically to a value around 35°. Iron, uranium, strontium, and barium behave somewhat differently in that the first two decrease to asymptotes around 25° and 28°, respectively, and the latter two show an increase in the critical angle.

Mach Stems in Aluminum, Barium, Lithium, Strontium, Thorium, Iron, and Uranium

The maximum pressure that can be attained behind the Mach stem is found from the intersection of the original polar with the ordinate marked as P_m in Fig. 16. P_{cr} and P_{nr}, respectively, represent pressure behind the regular reflection at the critical angle and pressure behind the normal to the reflected shock.

Comparing pressures P_m, P_{cr}, and P_{nr} at the critical angle, one could see that all materials behave differently and, depending on the strength of the initial shock, critical conditions may be those resembling all three cases. Figures 18 through 24 illustrate this effect for each material separately. In each figure P_m, P_{cr}, and P_{nr} are normalized with P_1 and plotted against that value. For the ranges shown, aluminum is found to yield types I and II, lithium and strontium will both give types II and III, and thorium seems to cover the complete range of type II, while iron and uranium will only yield type I and barium only yields type III.

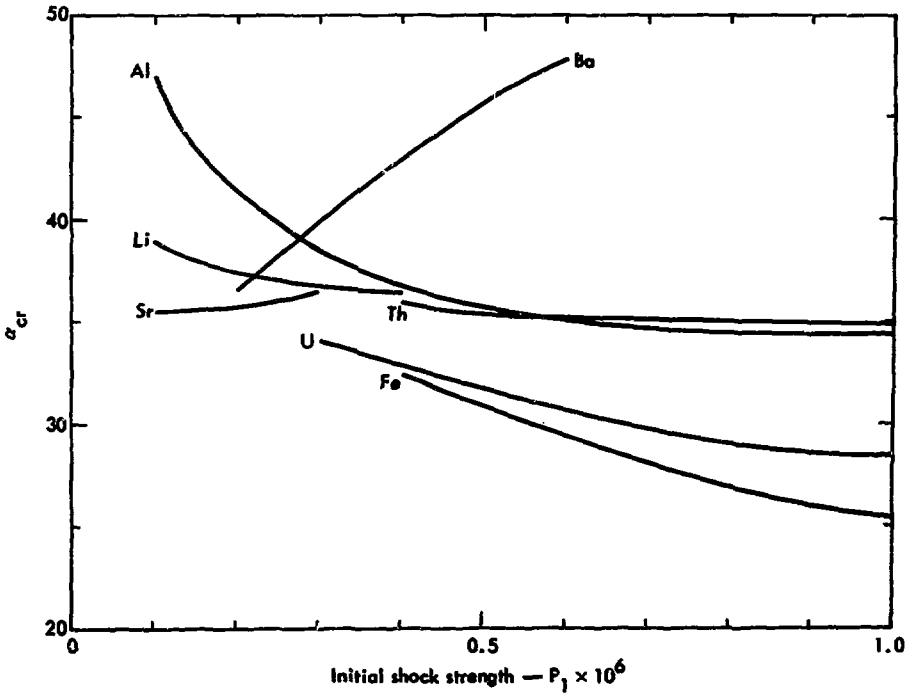

Fig. 17. Critical angle α_{cr} vs initial strength of interacting shocks for all investigated materials.

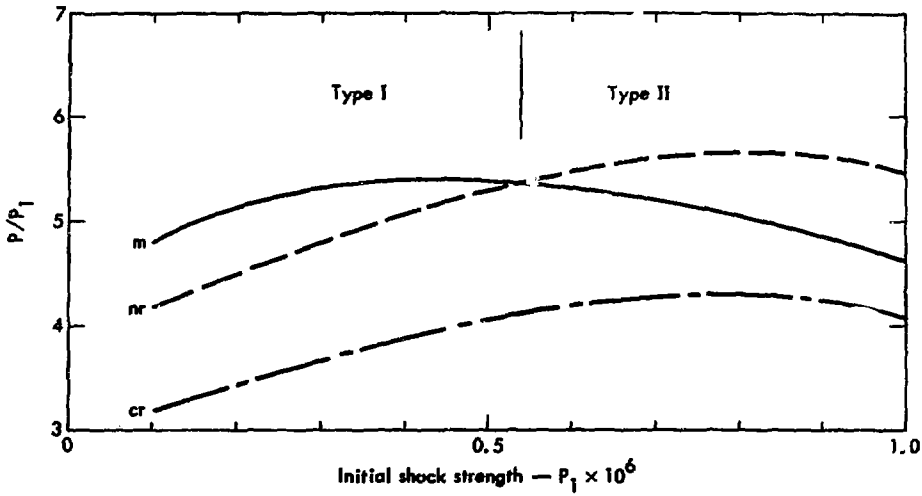

Fig. 18. Critical pressure ratios vs initial shock strength in aluminum.

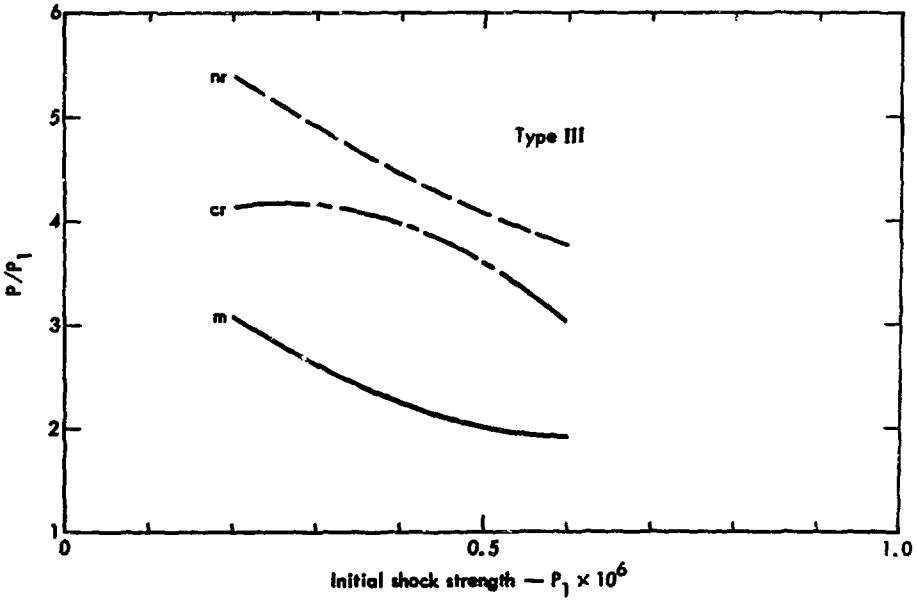

Fig. 19. Critical pressure ratios vs initial shock strength in barium.

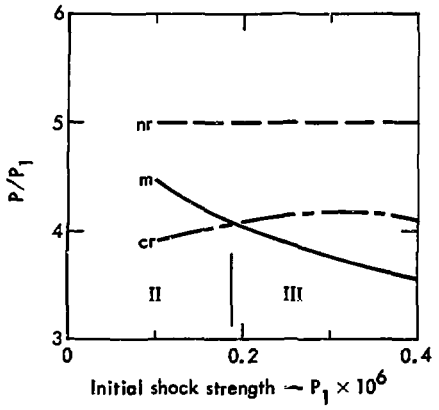

Fig. 20. Critical pressure ratios vs initial shock strength in lithium.

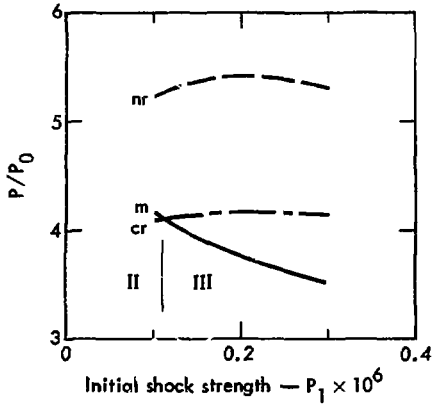

Fig. 21. Critical pressure ratios vs initial shock strength in strontium.

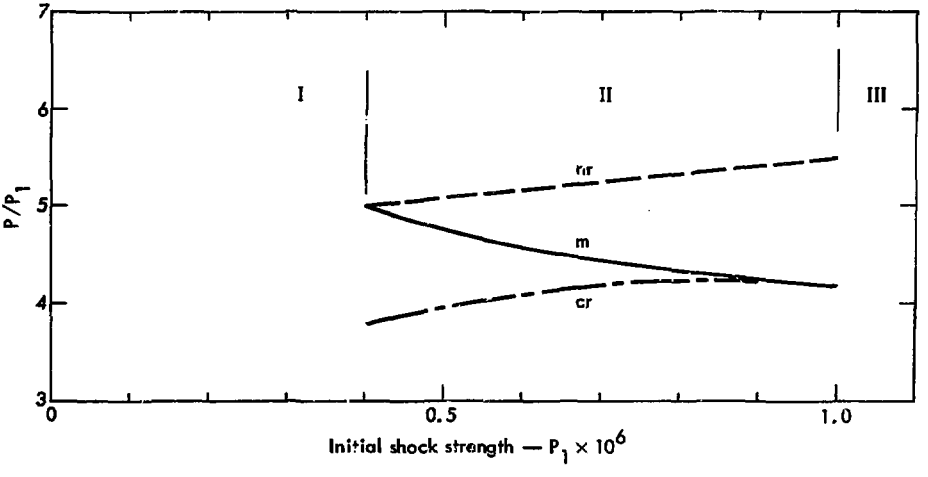

Fig. 22. Crtical pressure ratios vs initial shock strength in thorium.

Also of interest is the effective increase of pressure with increase in the initial shock strength. While in most materials the ratio P_m/P_1 decreases with P_1 or stays nearly constant (as in aluminum and uranium), in iron it again behaves differently and increases to over an eight-fold pressure jump at $P_1 = 10^6$ ($p_1 = 1$ Mbar). Thus, even though the maximum Mach stem pressure P_m is found in iron, its rather strong display of type I diminishes the effectiveness of

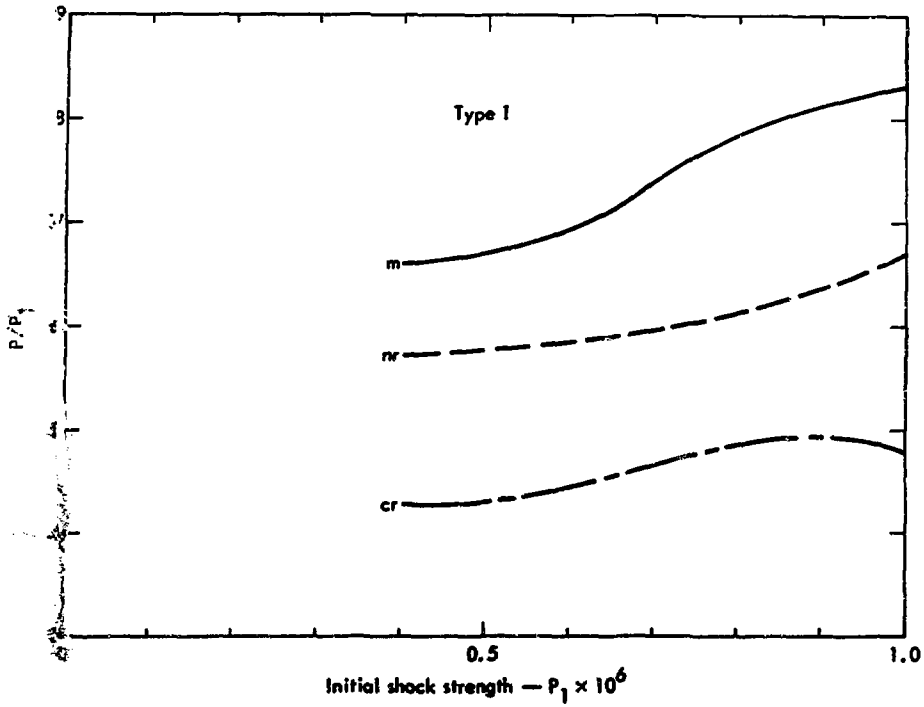

Fig. 23. Critical pressure ratios vs initial shock strength in iron.

a clear Mach stem and its potential in vaporizing a quantity of this material.

Using the present graphical technique one can also determine the range of pressures attainable in a certain material with a particular shock strength as the angle of incidence is varied. Assuming that the most realistic solution is the one that yields the lowest pressure, one can determine the whole range of angles that yield a possible solution. For the purpose of illustration, such analysis has been carried out for three different types of critical reflection, and the results are shown in Figs. 25, 26, and 27. While there is a big pressure jump from a regular reflection to a Mach stem in types I and II, in type III the Mach stem solution takes over before regular reflection meets its limit, and therefore no pressure jump occurs in this case. Maximum pressure is always obtained near the critical condition. The further the angle is from the critical value, the lower is the pressure that is obtained from the reflection. Thus, in order to get maximum compression of a material, one must operate very close to the critical angle.

To illustrate how much entropy is gained by a Mach stem, an example is worked out for a series of collision angles for each material. In each case the initial

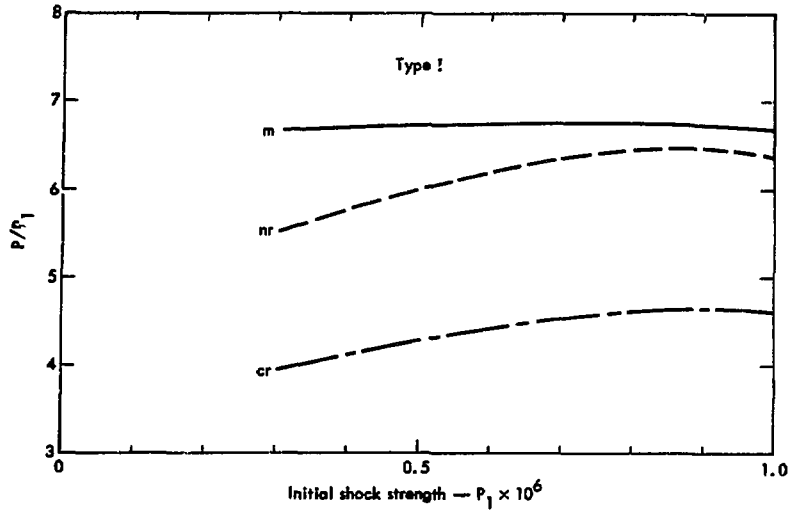

Fig. 24. Critical pressure ratios vs initial shock strength in uranium.

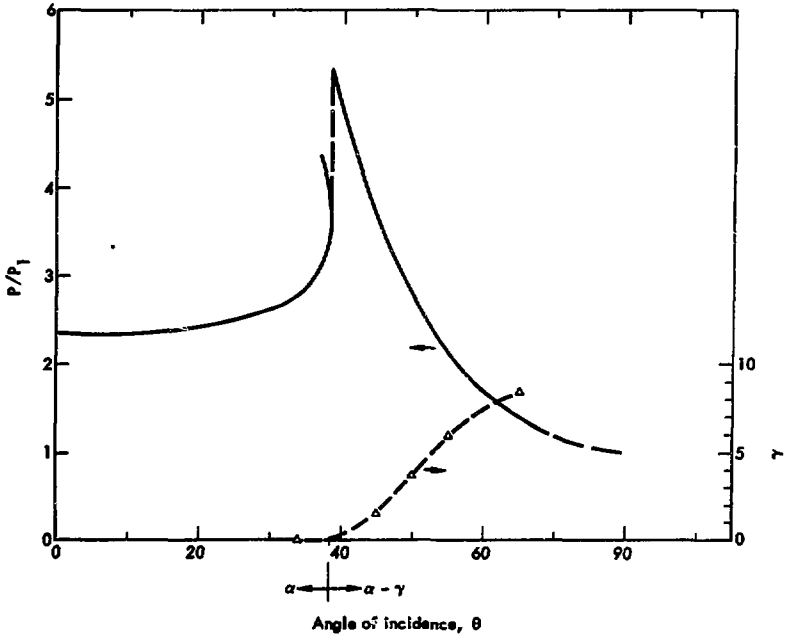

Fig. 25. Variation of the reflected pressure with incident angle θ in aluminum when p_1 = 300 kbar, values of δ taken from Ref. 18.

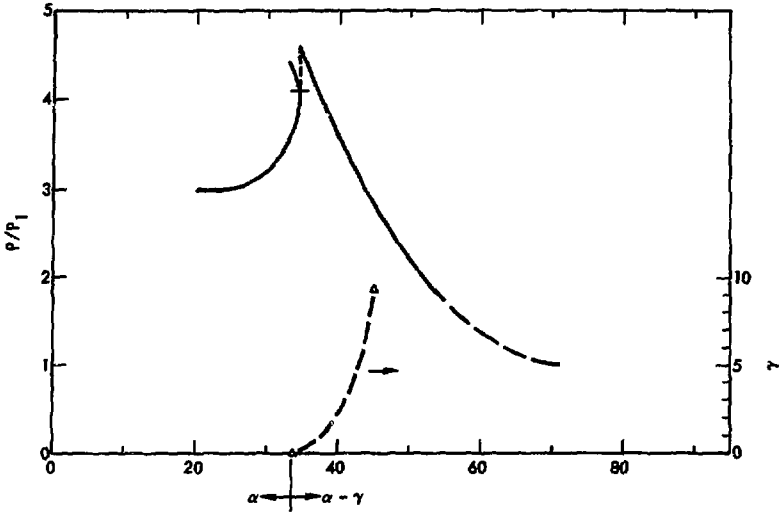

Fig. 26. Variation of the reflected pressures with incident angle θ in aluminum when p_1 = 1 Mbar, value of δ taken from Ref. 18.

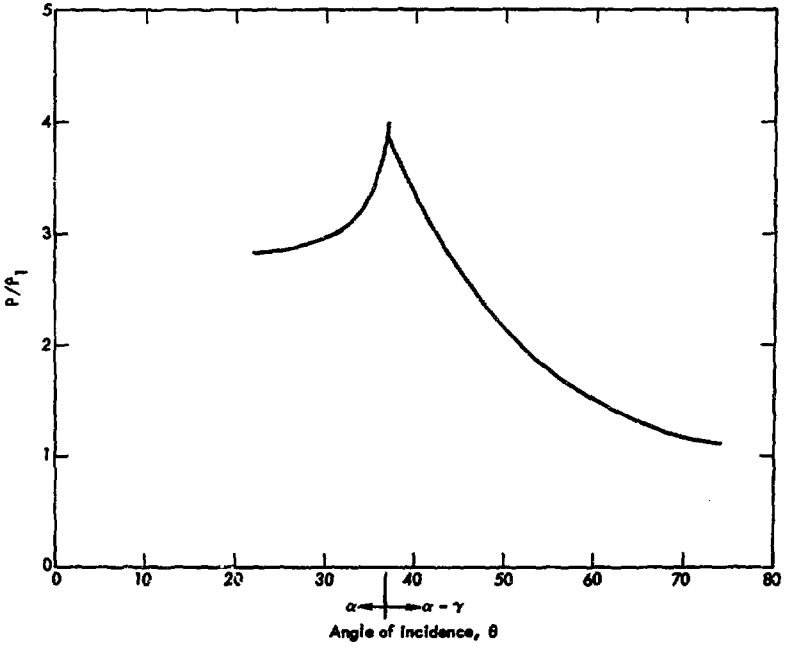

Fig. 27. Variation of the reflected pressures with incident angle θ in lithium when p_1 = 250 kbar.

shock was taken to be of different strength, but always one that was attainable with the same explosive-in-contact geometry.

In Figs. 3(a)-9(a) these initial shock strengths are indicated by a cross, and the final states behind the Mach stem are indicated by arrows with corresponding values of the incidence angle. The results clearly indicate that one can profit from a Mach stem design in getting a considerable gain in entropy, but it is also evident that an "in-contact" geometry, even one as strong as the octal-dural 400 system used in these examples, will not suffice for vaporizing material upon release, and for all materials except strontium and barium a stronger shock generating system is necessary.

Estimate of the Mach Stem Size

Before using the above criterion for practical application, one must consider one more factor of the problem: the amount of material that can be compressed to such high pressures; i.e., the amount of material affected by the Mach stem as compared to the total amount of material used.

Geometrically speaking, with reference to Fig. 1(b) one would be interested in knowing how large an angle γ one can get during such an interaction. In the present analysis we do not attempt to predict the angle γ. We expect that this calculation and/or experiment could be profitably investigated in the future.

From the experimental data available in the literature, one finds that at critical conditions the angle γ is extremely small and increases very slowly with deviation from the critical angle α. Therefore, the gain in compressed substance is a trade-off to the amount of compression, and the practical problem of inducing large quantities of vapor becomes one of determining the optimal geometry. If one could speculate on the basis of data available, the angle γ grows much more rapidly with stronger shocks than with weaker interactions, as is indicated by the dashed curves on Figs. 25 and 26, which were plotted through experimental points taken from Ref. 18. It seems feasible that with stronger shocks one could increase the size of the Mach stem to compress a noticeable amount of the material.

As an estimate of how much material one can expect to compress with a Mach stem at higher initial pressures, one can use the experimental data of Ref. 18 shown in Fig. 26. At $\alpha = 45°$ we find that $\gamma = 9°$, and there still is a significant pressure increase of $P_m/P_1 \approx 2.3$. Such a system is represented geometrically in Fig. 28; from the figure it follows that the amount of material affected by the Mach stem as compared to the total is

$$\frac{x}{y} = \frac{L\tan 9°}{L\tan 45°} = 0.158 \approx 15\%.$$

If other materials behave in a similar way, then with stronger initial shock one can expect the Mach stem to cover 10-20% of the original material.

In the above analysis we have only described a system in which two plane waves interact at an oblique angle α. It is also possible to obtain Mach stems in other configurations where theoretical

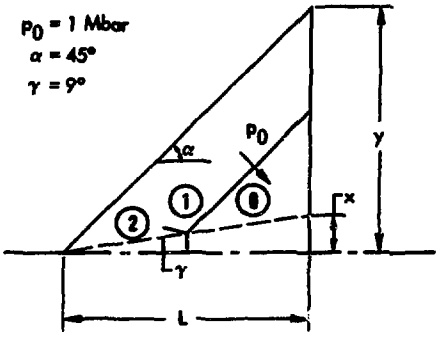

Fig. 28. Geometrical representation for the estimate of efficiency.

analysis is more difficult. Another such system has been described by Fowles and Isbell[24] in which a cylindrical block is surrounded by high explosive. A detonation wave propagates along the high explosive, and a conical shock wave is induced in the material. A Mach stem forms in the sample cylinder near the apex of the cone. In this case the angle of the cone will originally depend on the relative impedance of the materials, but it can also be varied by reshaping the material from a straight cylinder to a cone. Due to the three-dimensional character of this problem, one can presumably improve on the efficiency of the system. In this geometry the maximum pressure behind the Mach stem will be limited by the strength of the original shock, which can be generated either by an "in-contact" explosive or by means of a conically or cylindrically imploding flyer plate.

Conclusions

In the present study we have examined the shock states that may be produced in various metals with available explosive systems. The entropies produced by shocks in porous and solid samples and the entropy required for vaporization are calculated, and the comparison is used as a quantitative guide to estimate the degree of vaporization for a given shock strength. Systems that optimize the trade-offs between the shock-induced particle velocity, the maximum specific entropy imparted by a shock, and the amount of material that receives sufficient entropy to induce vaporization could be designed using as references the present analyses of shock dynamics and the calculation of shock-induced thermodynamic state.

Both plane-wave and Mach-stem shock systems are capable of inducing vaporization of aluminum, iron, strontium, barium, and thorium. Only Mach-stem shocks are capable of vaporizing lithium and possibly uranium. Plane-wave techniques, because of their inherent efficiency in transferring internal energy to a large quantity of metal, appear to be the most promising techniques for use on the first four metals even though substantial vaporization probably cannot be achieved, except possibly in the case of strontium and barium.

Specifically, we find for the plane-wave case that for a given explosive system, such as a flyer-plate launching device, a certain initial porosity provides the optimum conditions for entropy production. For the case of aluminum,

distentions of 1.6, 1.7, or 1.8 are optimum for 4- or 5-km/sec iron and tungsten flyer plate impacts. For iron the optimum distention of the sample is about 1.6 or 1.7. For thorium, initial distentions of ~2.0 will probably induce maximum, but incomplete, vaporization. As a result of the investigation of plane-wave shock vaporization, we concluded that both uranium and lithium required convergent, and possibly Mach-stem, flow to induce significant vaporization. In this latter geometry, a fraction (we estimate 20%) of the sample can be vaporized.

Investigating the conditions that are required to induce Mach stems in the same materials, we found that the collision of two shock waves at an oblique angle does not always result in a clean Mach stem. The Mach-stem formation depends on both the equation of state of the material and on the strength of the initial shock. Within the range of initial pressures that are easily attainable by conventional high explosive systems, barium, lithium, and strontium will propagate clean Mach stems. Thorium and aluminum will propagate Mach stems for shocks above 400 and 510 kbars, respectively. Iron and uranium, although behaving in a similar fashion, do not readily form a clean triple wave intersection. Additional compression takes place between the reflected wave and its Mach stem for these metals.

Pressurewise, iron and uranium are the most interesting materials, since Mach stems can produce pressures 6 to 8 times those of the initial shock. Aluminum, lithium, strontium, and thorium yield four- to five-fold increases in shock pressure, while barium gives no more than a three-fold pressure increase. The angles required to induce a series of specific entropies for various Mach-stem geometries are presented in graphical form for system design proposes.

Acknowledgments

We appreciate the discussions with R. N. Keeler, E. B. Royce, and N. Rosenberg (AFCRL) concerning this problem. D. Young's help with our analyses of the thermodynamics of the liquid-vapor region and F. Rogers' help in obtaining data for barium and strontium are appreciated.

References

1. Y. B. Zeldovich and Y. B. Raizer, Physics of Shock Waves and High-Temperature Hydrodynamic Phenomena, Vol. II (Academic Press, New York, 1967).
2. M. H. Rice, R. G. McQueen, and J. M. Walsh, "Compression of Solids by Strong Shock Waves," Solid State Physics 6, 1063 (1958).
3. J. M. Walsh and R. H. Christian, "Equation of State of Metals from Shock-Wave Measurements," Phys. Rev. 97, 1544 (1955).
4. R. Grover, R. N. Keeler, F. J. Rogers, and G. C. Kennedy, "On the Compressibility of the Alkali Metals," J. Chem. Phys. 30, 2091 (1969).
5. G. T. Furukawa and T. B. Douglas, "Heat Capacities," in American Institute of Physics Handbook, D. E. Gray, Ed. (McGraw-Hill, New York 1963). pp. 4-47.
6. R. G. McQueen, S. D. Marsh, J. W. Taylor, J. N. Fritz, and W. J. Carter, "The Equation of State of Solids from Shock Wave Studies," in High-Velocity Impact Studies, R. Kinslow, Ed. (Academic Press, New York, 1970), p. 294.
7. R. Hultgren, R. L. Orr, P. D. Anderson, and K. K. Kelly, Selected Values of the Thermodynamic Properties of Metals and Alloys (John Wiley & Sons, New York, 1963), also revision (1970).
8. R. C. Weast, Handbook of Chemistry and Physics (The Chemical Rubber Co., Cleveland, 1969).
9. D. R. Stull, JANAF Thermochemical Tables, The Thermal Research Laboratory, Dow Chemical Corp., Midland, Mich.; Clearinghouse for Federal Scientific and Technical Information, Washington, D. C., PB 168-370 (1965).
10. D. Young and B. Alder, "Critical Point of Metals from the van der Waals Model," Phys. Rev. A 3, 364 (1971).
11. D. J. Andrews, Equation of State of the Alpha and Epsilon Phases of Iron, Ph.D. Thesis, Washington State University (1970).
12. G. D. Anderson, D. G. Doran, and A. L. Fahrenbruch, Equation of State of Solids: Aluminum and Teflon, Stanford Research Rept., Air Force Weapons Laboratory Technical Rept. 65-14M (December 1965).
13. A. S. Balchan and G. R. Cowan, "Method of Accelerating Flat Plates to High Velocity," Rev. Sci. Instr. 35, 937 (1964).
14. R. G. McQueen and S. P. Marsh, "Equation of State for Nineteen Metallic Elements from Shock-Wave Measurements to Two Megabars," J. Appl. Phys. 31, 1253 (1960).
15. F. Rogers, Lawrence Livermore Laboratory, private communication.
16. M. H. Rice, "Pressure-Volume Relations for the Alkali Metals from Shock-Wave Measurements," J. Phys. Chem. Solids 26, 483 (1965).
17. R. Courant and K. O. Friedrichs, Supersonic Flow and Shock Waves (Interscience, New York, 1948).

18. L. V. Al'tshuler, S. B. Kormer, A. A. Bakanova, A. P. Petrunin, A. I. Funtikov, and A. A. Gubkin, "Irregular Conditions of Oblique Collision of Shock Waves in Solid Bodies, Sov. Phys. JETP 14 (5), (1962).

19. J. Leygonie and J. Cl. Bergon, "Détermination du Coefficient de Grüneisen en Fonction du Volume Spécifique par L'étude du Phénomène de Réflexion de Mach," Proc. Symposium on Behaviour of Dense Media under High Dynamic Pressure (International Union of Theoretical and Applied Mechanics, Paris, 1967) p. 160.

20. P.L. de Beaumont and J. Leygonie, "Vaporizing of Uranium after Shock Loading," Fifth International Symposium on Detonation (Pasadena, Calif., 1970).

21. A. K. Oppenheim, J. J. Smolen, and L. J. Zajac, "Vector Polar Method for the Analysis of Wave Intersections," Comb. Flame 12 (1), 63 (1968).

22. A. K. Oppenheim, J. J. Smolen, D. Kwak, and P. A. Urtiew, "On the Dynamics of Shock Intersections," Fifth International Symposium on Detonations (Pasadena, Calif., 1970).

23. P. Laharrague, J. Morvan, and J. Thouvenin, "Réfraction d'une Onde de Choc," and Proc. Symposium on Behavior of Dense Media under High Dynamic Pressure (International Union of Theoretical and Applied Mechanics, Paris, 1967).

24. G. R. Fowles and W. M. Isbell, "Method for Hugoniot Equation-of-State Measurements at Extreme Pressures," J. of Appl. Phys. 36 (4), 1377 (1965).

Appendix

ENT, a Fortran IV Program for Calculating Entropy and Shock States in Solid and Porous Metals

I case = control No. ; for I case = 1 or 2 continue
for I case = 3 stop

IP = No. of pressures along principal Hugoniot

SUBST = material being calculated

THETO = Debye temperature, STP

GAMO = Grüneisen ratio, STP

MBAR = mean atomic weight

RHOO = density, STP

PH(I) = principal Hugoniot pressure

TH(I) = principal Hugoniot temperature

UP(I) = principal Hugoniot compression

GA(I) = principal Hugoniot/Grüneisen ratio

I = index point on principal Hugoniot

J = index of porosity

M = distention ratio

P(I,J) = shock pressure

U(I,J) = particle velocity

S(I,J) = entropy

TPOR(I,J) = temperature porous Hugoniot

FEUP = polynomial coefficients for shock particle velocity—pressure (U_s - P) relation for iron

WUP = polynomial coefficients (U_s - P) for tungsten

ALUP = polynomial coefficients (U_s - P) for 2024 aluminum

FEU = shock particle velocity points, Hugoniot

FEP = shock pressure points, Hugoniot

```
//ENT    JOB (64516,TJA,SL),'THOMAS J. AHRENS'
//      SET   PRT=6
//      SET   PLT=60
//         EXEC  FORTG
//FORT.SYSIN DD *
      PF(X,A1,A2,A3,A4)=A1+ A2*X + A3*X*X + A4*X**3
      DOUBLE PRECISION STOR(4,11)
      DIMENSION  FEU(8),FEP(8),DATA(3,8),FEUP(4),WUP(4),ALUP(4)
     1,FT(3,4),TN 4),SV(4),FR(4) ,R(9,6),SVV(4,6),TMM(4,6)
      DIMENSION VPP(6,5),STT(6,5)
      DIMENSION SUBST(4),VP(9),PH(9),GA(9),TH(9),TE(9),TP(9),DATS(3,10)
     1,S(9,6),TPOR(9,6),U(9,6),X(160) ,DD(3),SQ(9) ,DAT(3,10)
      DATA  WUP/.20996E-11,.76733E0,.27650E0,-.34697E-1/
      DATA  ALUP/-.6378E-2,.15459E0,.36446E-1,-.242876E-3/
      DATA  FEU/ 0.,.55,.95,1.29,1.58,1.85,2.46,2.95/
      DATA  FEP/ 0.,.2,.4,.6,.8,1.,1.5,2.0/
      C= 4.187E7
      REAL  MBAR ,M
  1   FORMAT(21I,4A4)
  2   FORMAT(1X,4A4)
  3   FORMAT(4F10.5)
  4   FORMAT(1X,'THETO =    ',F9.4,'GAMO =    ',F9.4,'MBAR =    ',F9.4,'RHO
     10 =    ',F9.4)
  5   FORMAT(4F10.5)
  6   FORMAT(1X,7X,' PH',19X,'TH',19X,'VP',19X,'GA')
  7   FORMAT(1X,4F20.10)
  8   FORMAT(1X,5X,I1,9X,I1,9X,F3.1,9X, F6.4,4X,F6.4,2X,      F7.1,4X,
     1F5.3,6X ,F5.1,6X,F5.3,6X,F5.2,6X,F9.1)
  9   FORMAT(1X,5X,'I',9X,'J',8X,'M',9X,'VP',9X,' P',12X,      'TH',9X,
     1'GA',9X,'TE',9X,'U',9X,'  S ',9X,'TPOR')
      DO 90 I = 1,160
 90   X(I) = FLOAT(I-1)*.1
C     ICASE=1,GAM(V);ICASE=2,GAMO ONLY
 2000 READ(5,1) ICASE,IP,SUBST
      DD(1)=SUBST(1)
      DD(2)=SUBST(2)
      WRITE(6,2)SUBST
      IF(ICASE.GT.2)  GO TO  1000
      READ(5,3) THETO, GAMO, MBAR,RHOO
      WRITE(6,4)THETO, GAMO, MBAR,RHOO
      READ(5,5) (PH(I),TH(I),VP(I),GA(I),I=1,IP)
      WRITE(6,6)
      WRITE(6,7)(PH(I),TH(I),VP(I),GA(I),I=1,IP)
      DO 50  I=1,IP
      P(I,1)=PH(I)
      U(I,1)=(((1./RHOO-VP(I)/RHOO)*PH(I))**.5 )*10.
      IF(ICASE.EQ.1) GO TO 80
      TE(I)= THETO*EXP(GAMO*(1.-VP(I)))
      GO TO 81
 80   TE(I) = THETO*EXP(GA(I)*            (1.-VP(I)))
 81   CONTINUE
      IF(ICASE.EQ.1)  GO TO 56
      GA(I)= GAMO*RHOO*VP(I)/RHOO
 56   CONTINUE
      TP(I)=.TE(I)/TH(I)
      T=TP(I)
      IF(TP(I).LT..1) GO TO  51
C     CALL ENT(T,ES)
C     S(I,1)= ES*C
      S(I,1)=24.94293/4.186*(ALOG(1./T)+1.3296+T*(3.22E-4+T*(2.4386E-2
     1 +T*(5.94299E-4+T*(-7.6243E-4+T*(9.3004E-5-T*3.84347E-6))))))
```

```
      GO TO 52
 51   S(I,1)=21.65 + ALOG(TH(I)/10./TE(I))*1.986*3.
 52   CONTINUE
      M=1.
      TPOR(I,1)= TH(I)
      DO 60  J=2,6
      M=M+ .2
      DP=PH(I)*(M-1.)/VP(I)/(2./GA(I)-M/VP(I)+1.)
        IF (DP.LE.0.) GO TO 63
      P(I,J)= PH(I)  + DP
      CALL DEBYE(T,CV,X)
      TPOR(I,J)=DP*VP(I)*MBAR/GA(I)/(CV*C)/RHOO/1.E-12 + TH(I)
      DS= 1.986*3.*ALOG(TPOR(I,J)/TH(I))
      S(I,J) = DS + S(I,1)
      U(I,J)=((1N/RHOO= VP(I)/RHOO)* P(I,J))**.5)*10.
 60   CONTINUE
      JT1=6
       GO TO 65
 63   JT1=J-1
 65   IF (I.EQ.1) JT=JT1
        IF (JT.GT.JT1) JT=JT1
 50   CONTINUE
      WRITE(6,9)
      DO 70  I=1,IP
      DO 71  J=1,JT
      M= 1.+ FLOAT(J-1)*.2
      WRITE(6,8) I,J,M,VP(I),
     1  P(I,J)          ,              TH(I),GA(I),TE(I),U(I,J),S(I,J),TPOR(
     2I,J)
 71   CONTINUE
 70   CONTINUE
      DO 801I=1,8
      DATA(1,I) = FEU(I)
      DATA(2,I) = FEP(I)
      DATA(3,I) = .1
 801  CONTINUE
      DATA(3,1) = .0001
 10   FORMAT(1X,'FEUP ARRAY'/4E20.7)
      CALL LSQUAR (DATA,8,4,FEUP,CH,STOR)
      WRITE(6,10)FEUP
      DO 61 I=1,4
      FT(1,I)=ALUP(I)
      FT(2,I)=FEUP(I)
 61   FT(3,I)=WUP(I)
      DO 701J=1,JT
      IPP = IP+1
      DATS(2,IPP) = 0.
      DATS(1,IPP) = 1.
      DATS(3,IPP) = .0001
      DAT(1,IPP) = 0.
      DAT(2,IPP) = 0.
      DAT(3,IPP) = .0001
      DO 711 I = 1,IP
      DAT(1,I) = U(I,J)
      DAT(2,I) = P(I,J)
      DAT(3,I) = .0001*FLOAT(I)
      DATS(1,I) = VP(I)
      DATS(2,I) = S(I,J)
      DATS(3,I) = .0001 *FLOAT(I)
 711  CONTINUE
      CALL  LSQUAR(DAT,IPP,4,TM,CH,STOR)
```

```
      CALL LSQUAR(DATS,JPP,4,SV,CH,STOR)
      DO 712  I= 1,4
      TMM(I,J) = TM(I)
  712 SVV(I,J) = SV(I)
  701 CONTINUE
CCCCC    FLYER PLATE TYPE
      DO 901I=1,3
      DO 91 J=1,4
   91 FP(J) = FT(I,J)
CCCCCCCC   POROSITY
      DO 93  K=1,JT
      DO 95 N = 1,4
      TM(N) = TMM(N,K)
   95 SV(N) = SVV(N,K)
      ILL= 10.*VP(IP)
      XMN = FLOAT(ILL)/10. -.1
      DO 156  NN= 1,IP
  156 SQ(NN) = S(NN,K)
      DO 196  KK=1,3
  196 DD(KK) =0.
      DD(3)=1.
   13 FORMAT(1X,9F11.5)
      WRITE(6,13)VP, SQ
CCCCCCCCCC      FLYER PLATE SPEED
      DO 92 J=1,5
      UFP = FLOAT(J)
      WRITE(6,12) TM, FP
   12 FORMAT(1X, 'TARGET PARAMETS' ,4E20.7/ 'FLYER PARAMETERS' ,
     1  4E20.7)
      CALL UPMAT(UFP,FP,TM,SU,   UT)
C     UFP= FLYER VEL.;FP= P-U FLYER FIT;TM= TARGET MAT P-U FIT;
C     S(U) PARAMETER FOR TARGET MAT.=SU
C     S FOR TARGET, U FOR TARGET
      RP = PF(UT,TM(1),TM(2),TM(3),TM(4))
      VPP(K,J)=1. + FLOAT(K-1)*.2 -UT*UT*RHO0*.01/RP
      VOL=VPP(K,J)
      STT(K,J)=PF (VOL,SV(1),SV(2),SV(3), SV(4))
      WRITE(6,11) J,UT,RP,VPP(K,J),STT(K,J)
   11 FORMAT(1X,'UFP =  ',I1,'     IMP M. PART. VEL.=',F10.5,'     P=',
     1 F10.5,'      REL VOL.= ', F10.5/'       ENT =',F10.5)
   92 CONTINUE
   93 CONTINUE
      DO 930 K=1,JT
      CALL MAXMIN(S(1,K),IP,YMX,YMN)
      IF (K.EQ.1) GO   TO 935
      IF (YMX.GT.YX) YX=YMX
      GO TO 930
  935 YX=YMX
      YN=YMN
  930 CONTINUE
      CALL MAXMIN(VP,IP,XMX,XMN)
      DO 945 K=1,5
      CALL MAXMIN (STT(1,K),JT,YMX,YMN)
      IF (YMX.GT.YX) YX=YMX
      CALL MAXMIN (VPP(1,K),JT,XM,XN)
      IF (XM.GT.XMX) XMX=XM
  945 CONTINUE
      CALL SCALE(YX,0.,TOP,BOTTOM,10,IER)
      CALL SCALE(XMX,0.,RIGHT,XLEFT,15,IER)
      CALL LABEL(0.,0.,XLEFT,RIGHT,15.,15,1H ,1,0)
      CALL LABEL(0.,0.,BOTTOM,TOP,10.,10,1H ,1,1)
```

```
      DO 950 K=1,JT
        ISYS=K-1
  950 CALL PLOTXY(1P,VP,S(1,K),XLEFT,RIGHT,BOTTOM,TOP,0,0,ISYS,1,DD)
      ISYS=5
      DO 1001 K=1,5
       ISYS=ISYS+1
       CALL PLOTXY(JT,VPP(1,K),ST(1,K),XLEFT,RIGHT,BOTTOM,TOP,0  ,0
     1 ,ISYS,1,DD)
 1001 CONTINUE
       CALL SYSEND(1,1)
  901 CONTINUE
      GO TO 2000
 1000 CONTINUE
      STOP
      END
      SUBROUTINE UPMAT(UFP,FP,TM,   ST,UT)
      DIMENSION ET(1,4),TM(4),      FP(4)
      DOUBLE PRECISION A(4),ROOTR(3),ROOTI(3),EPS
    1 FORMAT(1X,6E18.9)
      A(4)=FP(1)-TM(1)+ FP(2)*UFP+FP(3)*UFP*UFP +FP(4)*UFP**3
      A(3)=-1.*(TM(2)+FP(2)+2.*UFP*FP(3)+3.*FP(4)*UFP*UFP)
      A(2)= FP(3)-TM(3)+3.*UFP*FP(4)
      A(1)=-1.*(TM(4)+ FP(4))
      WRITE(6,1) A
       EPS=1.D-10
      CALL ROOT(A,3,ROOTR,ROOTI,EPS)
      WRITE(6,1) ROOTR,ROOTI
      DO 10 I=1,3
      R=ROOTR(I)
      IF(R     .LT.0.) GO TO 10
      IF(R     .GT.UFP) GO TO 10
      TEST=  TM(2)+ 2.* TM(3)*R +3.*TM(4)*R*R
      IF(TEST.LT.0.) GO TO 10
      TEST= -FP(2)-2.*FP(3)*(UFP-R)+FP(4)*(-2.*UFP**2+2.*R*UFP-UFP**2
     1+4.*R*UFP-3.*R*R)
      IF(TEST.GT.0.) GO TO 10
      UT =R
   10 CONTINUE
      RETURN
      END
      SUBROUTINE DEBYE(THTEE,CVE,X)
       DIMENSION X(160),   CV(160)
       DATA  CV                / 5.955,5.95,5.94,5.93,5.91,5.88,5.85,5.81,
     .77,5.72,5.670,5.61,5.55,5.48,5.41,5.34,5.26,5.18,5.09,5.01,
     24.918,4.83,4.74,4.64,4.54,4.45,4.35,4.25,4.15,4.05,3.948,3.85,
     33.75,3.65,3.56,3.46,3.36,3.27,3.18,3.09,2.996,2.91,2.82,2.74,
     42.65,2.57,2.50,2.42,2.34,2.27,2.197,2.13,2.06,1.99,1.93,1.87,
     51.81,1.75,1.69,1.63,1.582,1.53,1.48,1.43,1.39,1.34,1.30,1.26,
     61.21,1.18,1.137,1.100,1.065,1.031,0.998,0.966,0.935,0.906,0.87o,
     70.850,0.823,0.798,0.774,0.750,0.727,0.704,0.683,0.662,0.642,
     80.623,0.606,0.588,0.570,0.552,0.537,0.521,0.507,0.492,0.478,0.465,
     90.452,0.439,0.427,0.415,0.404,0.394,0.383,0.373,0.363,0.353,0.345,
     10.335,0.324,0.319,0.310,0.303,0.295,0.287,0.280,0.273,0.267,0.260,
     20.254,0.248,0.242,0.237,0.231,0.226,0.221,0.216,0.211,0.206,0.202,
     30.197,0.193,0.188,0.184,0.180,0.176,0.172,0.169,0.165,0.162,0.159,
     40.155,0.152,0.149,0.146,0.143,0.140,0.137,0.135,0.132,0.130,0.127,
     50.125,0.122,0.120,0.118,0.116/
      N = 160
      IF(THTEE.LT.X(1)) GO TO 10
      IF(THTEE.GT.X(N)) GO TO 10
      GO TO 13
```

```
10    WRITE (6,11)
11    OFORMAT(76H THE VALUE OF THTEE IS OUTSIDE THE RANGE OF X VALUES OF
     1          THE TABLE )
      GO TO 12
13    CONTINUE
      NINT = 4
      I=1+INT(10.*THTEE+.9999999)
   30  CONTINUE
      IF (I.GE.3) GO TO 40
       K=1
      GO TO 4
 40    IF(I.GE.158) GO TO 50
      K=I-2
      GO TO 4
 50     K=157
4     CALL XINTP (THTEE,X(K),CV(K),NINT,CVE)
12    RETURN
      END
      SUBROUTINE XINTP(ABSCIS,X,Y,N,VALUE)
C     AITKEN,S ALGORITHM IS USED FOR N POINTS INTERPOLATION
C
C
C     ABSCIS = ABSCISSA AT WHICH THE VALUE OF THE FUNCTION IS DESIRED
C     X = ARRAY OF ABSCISSA
C     Y = ARRAY OF ORDINATES -- THE VALUE OF THE FUNCTION AT THE ABSCISSA
C     N = THE NUMBER OF POINTS WE WISH TO USE FOR INTERPOLATION
C     N IS SET FOR A MAXIMUM OF 20
C     THE VALUE OF THE FUNCTION AT ABSCIS
C
C     THE BEST RESULT IS OBTAINED WHEN ABSCIS FALLS IN THE INTERVAL THAT
C     HAS EQUAL NUMBER OF POINTS ON BOTH SIDES
C
      DIMENSION X(20),Y(20),Z(20),XL(20,20)
      KK = N - 1
      DO 1 I = 1,N
    1 Z(I) = Y(I)
      K = 2
      DO 2 I = 1,KK
      DO 3 J = K,N
    3 XL(I,J) = Z(I) + (Z(J) - Z(I))/(X(J) - X(I)) * (ABSCIS - X(I))
      DO 4 JJ = K,N
    4 Z(JJ) = XL(I,JJ)
    2 K = K+ 1
      VALUE = Z(N)
      RETURN
      END
//SYSPLTDN    DD SYSOUT=N
//DATA   DD    *
28ALUMINUM
350.        2.          26.98       2.702
.1          374.        .9039
.2          508.        .8424
.3          707.        .7980
.4          968.        .7636
.5          1268.       .7358
.75         2290.       .6839
1.          3540.       .6472
1.2         4684.       .6244
29  IRON
175.        1.690       55.847      7.850
.2          416.        .8803
```

```
.4          657.        .8215
.6          1007.       .7829
.8          1444.       .7544
1.2         2523.       .7317
1.6         3812.       .6827
2.          5264.       .6588
2.4         6846.       .6388
2.7         8107.       .6256
14  BARIUM
110.                    137.34      3.51
.051        1035.       .665        1.343
.102        2329.       .581        1.27
.303        9457.       .472        1.146
.504        17918.      .432        1.093
3  END OF DATA
//
```